EXPERIMENTAL STUDY OF CURRENT RIPPLES USING MEDIUM SILT

by

ROBERT ANTHONY GRAZER

B. S. Geology
B. S. Geophysics
Boston College
(1980)

SUBMITTED IN PARTIAL FULFILLMENT
OF THE REQUIREMENTS OF THE
DEGREE OF

MASTER OF SCIENCE IN
GEOLOGY

at the

MASSACHUSETTS INSTITUTE OF TECHNOLOGY

June 1982

Signature of Author _____
Department of Earth and Planetary Sciences
June 30, 1982

Certified by _____
J. B. Southard
Thesis Supervisor

Accepted by _____
Undgren
T. Madden
Chairman, Department Committee

EXPERIMENTAL STUDY OF CURRENT RIPPLES USING MEDIUM SILT

by

ROBERT ANTHONY GRAZER

Submitted to the Department of Earth and Planetary Sciences on June 29, 1982 in partial fulfillment of the requirements for the Degree of Master of Science in Geology

ABSTRACT

A series of flume runs using medium silt devoid of clay minerals indicate that absence of ripples in fine sediments is due to increased cohesiveness of the finer grains due to interparticle ionic interactions involving clay minerals. Runs were conducted in a 10 m long recirculating flume of width 15 cm, using silt of mean size 20.5 μm and a water-sucrose solution varying in kinematic viscosity from 1 to 10.5 cS, providing Reynolds-Froude scale model ratios up to 4.8. Two runs with a sand of mean size 115 μm proved the validity of the Reynolds-Froude scale modeling technique in scaled-up situations. Ripples were examined in sediment of effective size 29 to 4 μm. [The lower value being extremely close to the silt-clay boundary of 3.9 μm.] The ripples behaved dynamically like ripples more commonly examined in coarser sediment. Triangular profiles with steep lee and gentle stoss slopes, scour at reattachment, and bed-load transport up the stoss slope with slumping at the brinkpoint were in evidence in all runs. Suspended sediment was abundant in all runs but ripple migration was due to bed load transport, although with increasing fluid viscosity, suspended sediment aided in ripple migration through particle fallout. Unusually large ripples found in nature could be attributable to fluids with anomalous viscosity due to effects of temperature or suspended sediment concentration. Glciolacustrine prodelta flows or density currents are flows capable of producing unusually large ripples.

Thesis Supervisor: Dr. John B. Southard, Professor of Geology

TABLE OF CONTENTS

LIST OF FIGURES

LIST OF TABLES

ACKNOWLEDGMENTS

I would especially like to thank my girlfriend of the past 8 years, Marion Rideout, for her support and encouragement throughout the experimental and writing stages of the thesis. Her willingness to roll up her sleeves and help while I was fixing and altering the flume as well as her aid in drafting many of the figures in the thesis was especially appreciated.

I also wish to thank fellow sedimentologists Roger Kuhnle and Chris Paola for their words of encouragement and wisdom gained from years of flume experience, Doug Walker for supplying the sand and on one occasion preventing the pump's self-destruction, and Dan Carey of Boston College for his interest in the project and aid in silt analysis. I am also grateful to Professor David Roy of Boston College for sparking my interest in sedimentology and Professor John Southard for his support and enthusiasm in seeing this project to its conclusion.

Finally I wish to thank my parents Anthony and Gertrude Grazer for their willingness to help and moral encouragement during difficult times as well as Marion's parents, James and Elizabeth Rideout for their moral support.

Financial support which allowed me to attend MIT was provided by the John Lyons Fellowship. The MIT department of Earth and Planetary Sciences Research Fund Committee helped underwrite a significant portion of the cost of the experiments.

INTRODUCTION

MOTIVATION

The primary incentive for conducting research is to explore areas in which either too little information is available to allow conclusions to be drawn from it or the information exists yet controversy abounds as to its meaning. In this study, the former is applicable as bedform investigations involving cohesionless sediment of mean size less than 100 μm are rare, less than ten studies in the past twenty years. Paradoxically, silt and finer particules comprise the principal load of most rivers as well as a major part of ocean bottom sediment. The major part of the earth's sediment, both consolidated and unconsolidated, is less than sand size. Thus silt research fills gaps in sedimentology and on the wider scale, geology in general.

Recent invironmental concerns focused attention on the paths of indiscriminately discharged particulate pollutants. As many of these pollutants end up in water, complete knowledge of their migration pathways is essential. This becomes more critical when it is understood that many of these particulate pollutants can be absorbed onto the surfaces of silt particles and transported great distances. Thus knowledge of silt transport properties for environmental reasons is essential as well.

Lastly, the applicability of a Reynolds-Froude modeling technique in scaled-up situations is tested

and used in the present research, providing easier and more detailed observation of ripples in fine sediment using laboratory geometrically and dynamically scaled-up ripples. This modeling technique allows for the observation of ripple dynamics in sediment less than 10 μm. This is significant since to date, only one study, that by Rees (1966), has been made with such fine sediment.

PRIOR WORK

A non-sedimentologist would regard the overwhelming wealth of data concerned with bedforms formed in sand as perplexing as the limited amount of data for bedforms in non-cohesive sediment less than sand size (63 μm). Absence of bedform research in silt may result not only from difficulties inherent in procuring sufficient quantities of cohesionless silt but also misunderstandings concerning stability of ripples in silt based on theoretical calculations made by Bagnold (1966). Bagnold suggested that ripples would not form in sediment of mean size less than 20 μm. His calculations suggested that when flow was capable of moving 20 μm grains, turbulence would be so great that grains would immediately become suspended, thus tractive bedforms such as ripples could not exist. Rees (1966) conducted incipient transport research on naturally laid 10 μm silt which did not appreciably disagree with Bagnold's results. From his observations on ripples, Rees concluded that ripples were

stable only in the presence of excess load in suspension. Without excess load, the bed became plane. Rees suggested therefore that ripples could not be stable in an equilibrium flow condition.

Harms (1969) noted that Bagnold's contention was paradoxical since ripple marks in silt-sized sediment existed in consolidated sedimentary deposits. Southard and Harms (1972) conducted flume studies using 2 silts of mean sizes 30 and 40 μm. They and subsequent investigators (Banerjee, 1977; jopling and Forbes, 1979) noted that ripples exist over a wide range of mean flow velocities and that with increasing velocity, contrary to bedform development in sands, ripples in silt were followed abruptly by a plane bed. Absence of a dune bed agrees with previous work by Southard (1971) which suggests that the dune field pinches out at a mean sidiment size of 80 μm. A ripple state followed abruptly by plane bed is borne out in subsequent experimental analyses (Banerjee, 1977; Southard and Harms, 1972; Jopling and Forbes, 1979).

Morphology of ripples in silt is similar to that in sand, the difference being that the slipface angle may be less than that found in sands (Harms, 1969). At low flow velocities, ripples have relatively continuous but somewhat sinuous crests, fairly uniform heights and lengths, planar lee slopes meeting crests and troughs at sharp angles, and erosional stoss slopes at the point of reattachment.

With increasing flow velocity, ripple height decreases and the ripple profile becomes more rounded. Jopling and Forbes (1979) noted that a hummocky type of ripple was common as well, consisting of an almost symmetrical longitudingal profile. Banerjee (1974) measured ripple migration rates obtaining values on the order of 0.001 cm/sec, which is the right order of magnitude based on studies of migration rate of sand ripples (Dillo, 1960).

DEFINITIONS

Due to the current proliferation of terms in the geological literature, important terms used in this study will be presented here. The most important definition, one for current ripples, is also the most difficult one.

Ripples are small-scale downstream-migrating bedforms, asymmetric in profile with gentle upstream stoss slopes (1-8^{o}) and steeper downstream lee slopes ($\simeq$30^{o}, Fig. 1). The steep lee-side portion approaches the angle of repose of the bed material. In profile ripples are characterized by their height and length (spacing). Allen (1968, 1970) suggests a semewhat arbitrary division of height, $H < 4$ cm and length $L < 60$ cm for differentiating ripples. For grain size $D < 200$ microns, Yalin (1977) suggests that ripple length $L \simeq 1000\ D$ and height $H \simeq 0.1\ L$. Ripple index L/H varies from 5 to 20 approximately. Ripples form over a wide range of flow velocities and mean sidiment sizes. They exist in fine silt to coarse sand,

FIGURE 1

PROFILE OF A RIPPLE MARK

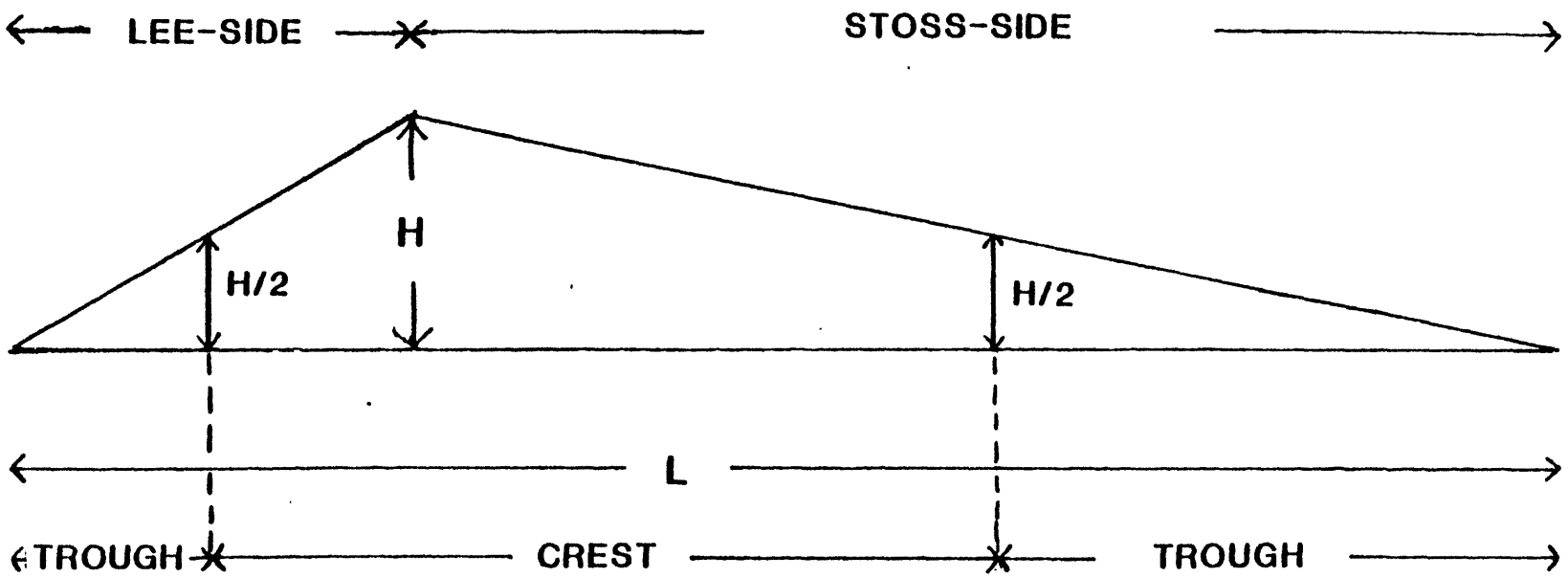

from 16 μm (Mantz, 1980) to 600 μm (Allen, 1968). Ripples tend to be two-dimensional at low flow velocities with sharply contacting stoss and lee slopes and become more three-dimensional with increasing flow velocity. They are stable in a wide range of flow conditions, with Reynolds numbers varying from 10^3 to 10^7 and Froude numbers commonly between 0.3 and 0.7. The free-surface profile is out of phase with the ripple configuration.

The following definitions were obtained from Allen (1968). In profile a ripple trough is defined as that portion of the ripple which relative to an imaginary trough line is less than one half the ripple height. A ripple crest exceeds one half the ripple height (Fig.]). Slipface is defined as the steeply sloping segment of the lee side built by avalanching and settling of grains.

In this paper, ripple height H is defined as the vertical distance between the trough immediately preceding the ripple and the highest point on the ripple crest (summitpoint). Ripple Spacing L (length, chord, or wavelength) is defined as the horizontal distance parallel to the flow between crests of two adjacent ripples. Migration rate is defined as the distance the summitpoint of a ripple travels downstream per unit time. Since ripples in the experiment were two-dimensional (except in Run 6) with crests extending across the full flume width transverse to flow, this definition of migration rate was easier to measure yet as effective as one requiring the migration of a ripple past some stationary marker.

EXPERIMENTAL ARRANGEMENT AND PROCEDURE

Equipment and Methods

The experiments were conducted in a recirculating flume 10 m long with a cross-section 15 cm wide and 30 cm deep(Fig. 2). Most of the channel of the flume is constructed of plywood three-quarter inch (1.9 cm) thick water-proofed by a coating of resin-saturated fiberglass mat. The observation area located approximately in the center of the flume has one half inch thick Plexiglas walls. Discharge was controlled by means of a gate valve located diwnstream of the pump outlet.

Due to the increased viscosity and density of the water-sucrose solution, several modifications were necessary in the flume. The motor for powering the centrifugal pump which drives the flow was increased from 2 horsepower to 3 horsepower due to the greater resistance of the water-sucrose solution. A larger diameter return pipe, 3 inches as compared to 2 inches, was installed to increase the flow discharge.

A point guage mounted on two 1-inch diameter steel rods located above the flume sidewalls was used to measure water surface slope S. A jack located beneath the flume at the downstream end allowed for the variation of flume slope, although flume slope was not altered in these experiments. A standard thermometer was used to measure fluid temperature throughout the runs.

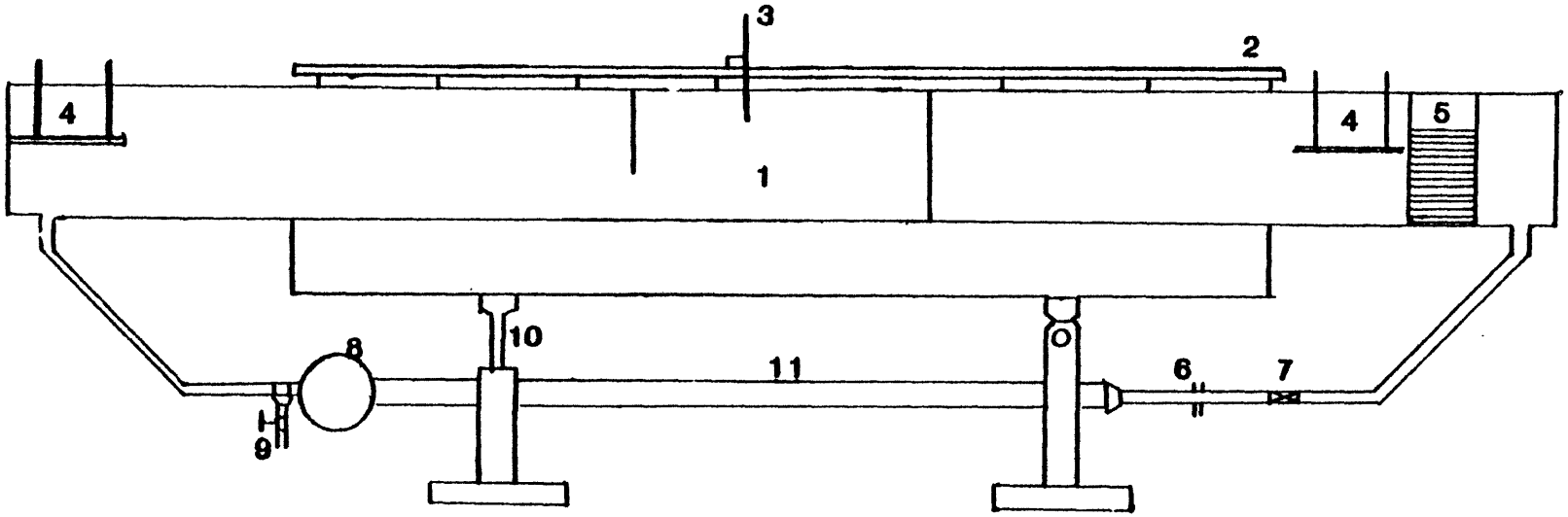

1 - OBSERVATION AREA

2 - INSTRUMENT RAILS

3 - POINT GAUGE

4 - WAVE DAMPERS

5 - FLOW BAFFLES

6 - ORIFICE METER

7 - GATE VALVE

8 - CENTRIFUGAL PUMP

9 - DRAIN

10 - TILTING JACK

11 - RETURN PIPE

FIGURE 2: Schematic of the 10 m long recirculating flume.

A calibrated U-tube mercury-water manometer connected to an orifice meter located in the return pipe was used to measure flow discharge. The manometer was calibrated by measuring the volume of water discharged per unit time for a wide range of pressure readings (Fig. 3). In order to test whether variation of water-sucrose solutions would affect discharge, a theoretical calculation was made which showed little difference in discharge due to variation of fluids used in these experiments (see Appendix 1).

Approximately one hundred 9-inch-long straws were stacked in orderly fashion then placed under compression just downstream of the flow inlet to help ensure fully developed turbulent flow. Adjustable-depth wave dampers constructed of two Plexiglas plates connected by threaded rods and held in place by nuts were installed downstream of the channel inlet and upstream of the channel outlet to help damp surface waves. Such waves were in evidence when the flume was turned on or shut off.

Suspended-sediment concentrations were determined by siphoning off twenty ml of fluid at mid-depth at the upstream and downstream ends of the flume, evaporating the samples to dryness, and weighing the resultant sediment. A twenty ml glass pipette with its end fashioned in a right angle was positioned with the end parallel to flow and facing upstream. Fluid was siphoned off at a velocity approximating the mean flow velocity. Sampling was performed over a 5 hour period (except in Run 6, 2.5 hours) with sampling at 15 minute intervals with the results

FIGURE 3: Graph of discharge vs mercury difference in the U-tube manometer.

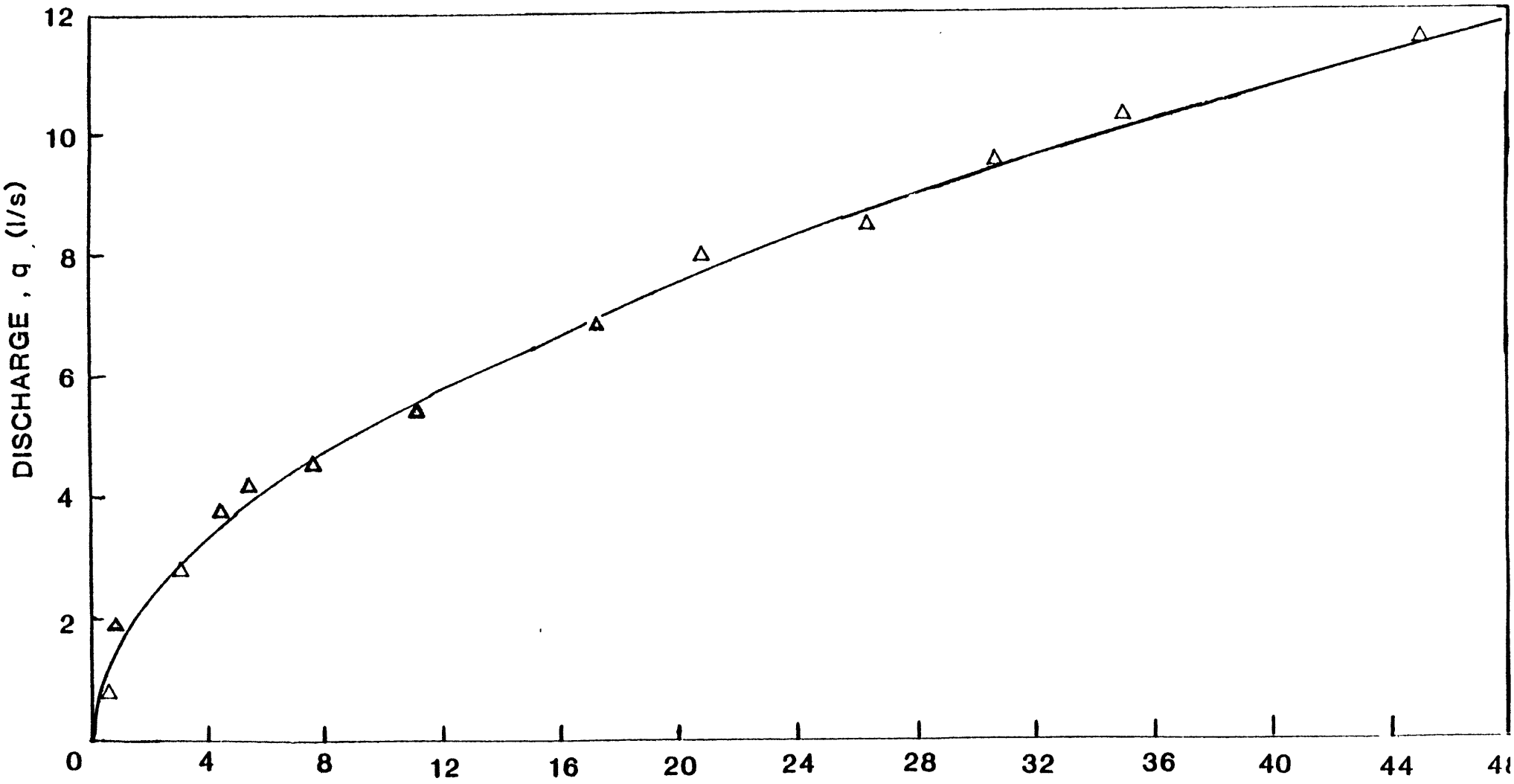
DISCHARGE , q (l/s)
12
10
8
6
4
2
0
4
8
12
16
20
24
28
32
36
40
44
MERCURY DIFFERENCE , ΔHg (cm)

averaged hourly. This procedure ensures that a representative sample of the sediment concentration is obtained, since most of the bedforms in Runs 1-6 required approximately one hour to migrate one ripple length. Samples obtained just downstream of the channel inlet represent average total sediment concentration because sediment discharges through the straws in a uniformly mixed condition. Samples downstream represent an average value of sediment in suspension because a fully developed suspended sediment profile exists at approximately 3 m downstream of the channel inlet.

A Bolex 16 mm movie camera with a time-lapse attachment was used to keep an accurate semi-continuous record of the runs. Depending on the run, two to four 150-watt spot lamps were placed above and below the observation section. The light were located such that contrast between ripples and flow was greatest. This was necessary since the high concentration of suspended sediment in the flow often made ripple observation difficult. Thirty-five mm pictures were also taken to provide more detailed pictures of interesting features, shapes, or structures. Film used in the Bolex movie camera was Kodak Tri-x reversal film (ASA 200), and filming rates varied from 6 frames per minute to one-half frame per minute. Thirty-five mm photos were taken using 35 mm Kodak Tri-x (ASA 400) and Pan-x (ASA 200) film.

Information obtained from the movie camera records included flow depth, ripple height, ripple length, lee-side angle, and ripple migration rate. Bed-load transport

rate was calculated using the average ripple volume, the average migration rate, and the submerged sediment weight. An average value of the submerged density of the silt, 1.33 gm/cm^3, was determined from measurements on silt obtained directly from the flume during runs.

Kinematic viscosity was the most important variable in the runs. It was necessary to measure the kinematic viscosity accurately as it provides for the scale ratios in the modeling technique. Kinematic viscosity of a fluid is dependent upon fluid viscosity, fluid temperature and sediment concentration. Thus it was necessary to measure this variable by taking samples during a run. Fluid samples were taken at mid-depth and the specific gravity of the solutions were determined using standard A.S.T.M. hydrometers.

The measurement of specific gravity allowed kinematic viscosity to be determined using the table for sucrose solutions contained in the CRC Handbook of Chemistry and Physics (Fig. 4). Accuracy of this method for determining viscosity was ensured by conducting fall-velocity experiments using particles with various densities in sucrose solutions with known discosities,(determined from the CRC Handbook). The viscosities of the solutions were then calculated using the vall-velocity of the particles according Stokes' Law of settling (Daily & Harleman, 1966).

FIGURE 4: Graph of specific gravity vs kinematic viscosity for sucrose-water solutions. Data from the CRC Handbook of Chemistry and Physics, 56th edition.

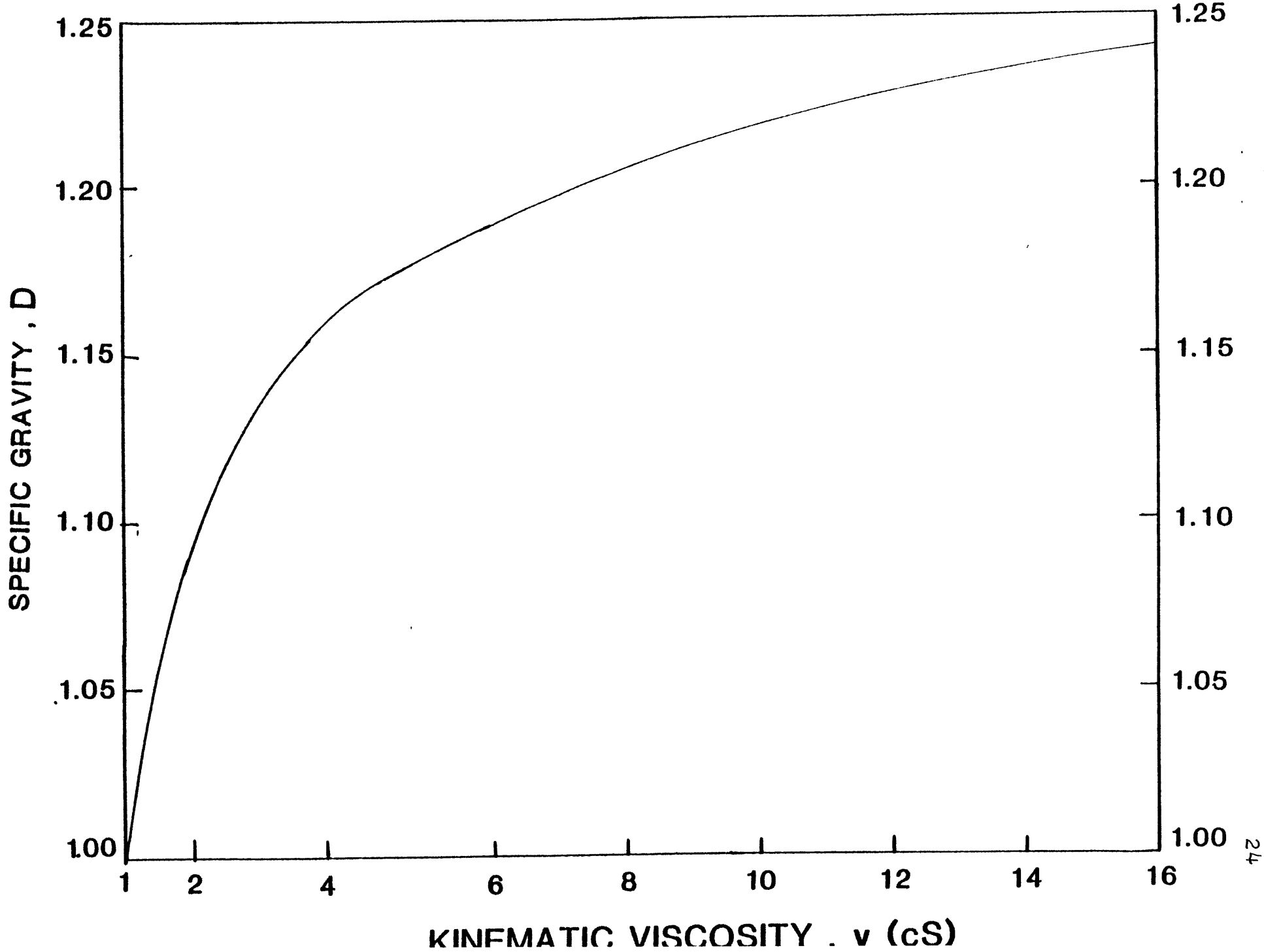
1.25
1.20
1.15
1.10
1.05
1.00
SPECIFIC GRAVITY , D
1
2
4
6
8
10
12
14
16
KINEMATIC VISCOSITY . v (cS)

SEDIMENT ANALYSIS

A fine sand and a medium silt were used in this study. The fine sand had a mean size of 115 μm and a sorting of 0.4 ϕ. It was well sorted, positively skewed, and mesokurtic (Fig. 5, Table 1). The sand was available in the laboratory from a previous study. To allow for the desired scale ratio of 4 in the Reynolds-Froude test runs, it was necessary to sieve the sand to finer sizes using large 2 ft. by 2 ft. box sieves. As displayed in Figure 7, the mean sizes of the scaled silt and sand agree favorably, although the sorting differs greatly between the two sediments. Mineralogically the sand consists of approximately 96% quartz, 2% feldspar, and 2% mica and heavy minerals. The sand grains are subrounded in shape. The sand was analyzed using standard 8 inch U.S. sieves at quarter-phi intervals and a Ro-tap sieve-shaking machine. Ten samples were individually sieved and the average of the ten was used to make the calculations shown in Table 1.

The medium silt had a mean size of 20.5 μm and a sorting of 1.2-1.5 phi. It was subangular in shape, poorly sorted, positively skewed, and platykurtic (Fig. 5, Table 1). The silt came from a loess deposit in Springfield, Illinois. Prior to use in these experiments, it had been sorted by differential settling in a wind tunnel with a resultant downwind size sorting. It was then further sorted by settling in large water tanks. Mineralogically, the silt consists predominantly of quartz with minor feldspar

FIGURE 5: Cumulative percent curves for the sand and silt.

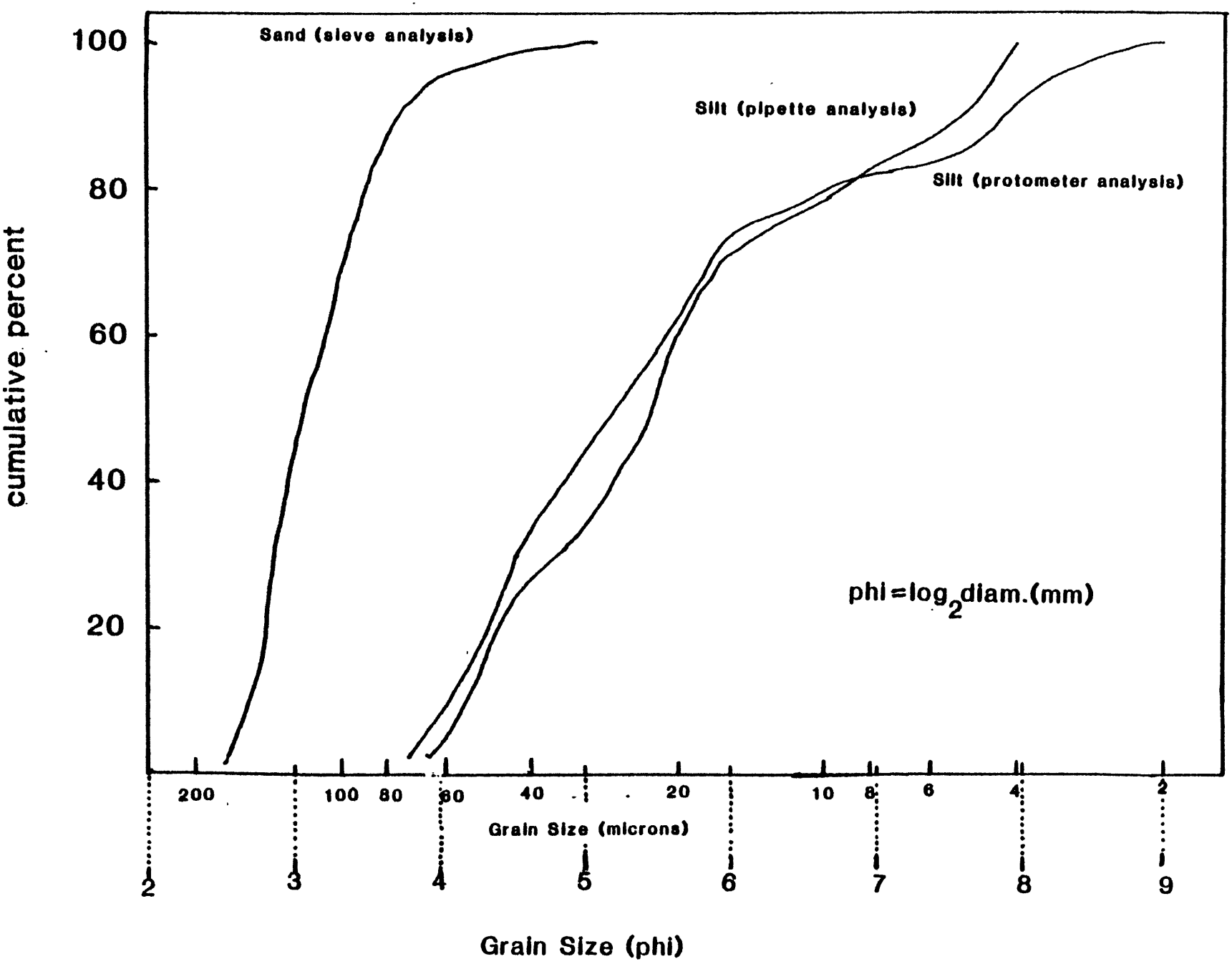
100
80
60
40
20
cumulative percent
Sand (sieve analysis)
Silt (pipette analysis)
Silt (protometer analysis)
phi=log2diam.(mm)
200
100
80
60
40
20
10
8
6
4
2
Grain Size (microns)
2
3
4
5
6
7
8
9
Grain Size (phi)

TABLE 1

Sediment Measurements

Descriptive Sediment Size Measures	Standard Sieve Analysis Sand ø (μm)	Pipette Analysis Silt ø (μm)	Prototron Particle Counter Silt ø (μm)
Folk Mean ($\bar{X}$)	3.1 (115)	5.6 (20.4)	5.6 (20.6)
Folk Median	3.1 (120)	5.4 (23.0)	5.3 (26.0)
Folk Inclusive Graphic Standard Deviation (SD)	0.4 (74)	1.2 (43.0)	1.5 (35.0)
Folk Inclusive Graphic Skewness	0.20	0.19	0.31
Folk Graphic Kurtosis	0.96	0.76	0.82

and dolomite rhombs. The silt is devoid of clay. The submerged density of the silt was measured on samples taken during runs and had an average value of 1.33 gm/cm^3.

The silt was analyzed using two different methods, the standard pipette analysis and a more recently developed method using a Prototron particle counter. As can be seen in Fig. 5, both methods yield similar results though it would appear that the particle-counter method is more accurate with finer sediment. The pipette analysis presented is the average of ten analyses while the particle-counter analysis is an average of three analyses. The pipette analysis method utilizes the differential settling velocities of grains due to variations in sediment size in accordance with Stokes' Law (Royse, 1970). The model ILI 1000 Prototron particle counter, located at Boston College, uses a laser and a photodetection system to count the number of suspended particles larger than a certain set size. It requires only an extremely small sediment sample and a complete analysis can be performed in less than twenty minutes.

Young (1975) observed that cohesiveness in fine sediment arises due to interparticle attractive forces, organic binding, and incipient cementation of particles, restricted to sediments with high carbonate concentrations. Mantz (1977) conducted experiments on sediment in the range 10-150 μm. He concluded that cohesiveness in silt is due to surface chemical attractive forces found on natural

silica solids due to an absorbed ferric iron surface. He also speculates that a minor amount of cohesiveness may be due to particle shape as angular particles may interlock.

In these experiments the silt demonstrated some cohesive behavior, and initially the ripples would not migrate. Since there were some algae in the flume, this resistance may have been due to organic binding, but even after several flushings of the fluid, the bedform resistance to movement persisted. Mantz (1977, 1980) noted that alteration of pH of the fluid affects the surface interactive forces and noted that in hard water, for D_{50} less than 100μm, the surface interactive effect is one of cohesion. Mantz noted that with a pH of approximately 8, or soft water, surface interactive effects are negligible.

The pH of the fluid in the flume was found to be about 5.5. Calgon (sodium hexa-metaphosphate), a commercial water softener, was added to the solution to raise the pH to 8. Calgon not only softens water but also acts to disperse suspensions, prevents precipitation of ferric hydroxide, and inhibits the formation of $CaCO_3$ (Boswell, 1961). Once the Calgon was added, transport of silt increased and the ripples began migrating.

Fluid

The Reynolds-Froude modeling technique used in these experiments requires a fluid which relative to water has

approximately the same density but a much higher viscosity. Also since it is desirable to vary the viscosity, it is desirable to choose a fluid which is soluble in water. For photographic considerations, a neutrally colored solution is required. To prevent flocculation, it is important that the fluid be ionically neutral.

Two liquids capable of fulfilling all these characteristics are water-sucrose mextures and glycerine-water mixtures. Refined sucrose was chosen because it is inexpensive and widely available.

One caution in using water-sucrose solutions is the importance of adding sufficient algicide to the solution, since water-sucrose plus light is an ideal growth medium for bacteria and algae. Such organic matter will not only mask the observation area but also can profoundly affect silt transport through the organic ginding of silt particles (Young, 1975). An equally important consideration is the maintenance of proper pH in the solution (Mantz, 1977). Mantz found that chemical surface interactive forces in sediment 10-150 μm in size are minimal in solutions with pH equal to 8. Mantz found that for D_{50} less than 100 μm, the effect in hard water solutions was that of cohesion. The water used for the sucrose solution had a pH of 5.5-6. In one trial run using the sucrose solution, ripple shapes developed but did not migrate over a period of two days.

Calgon, a commercial water softener, was then added to the fluid to soften the water to a pH of 8. Ripples began migrating less than 20 minutes after addition of Calgon. Thus proper maintenance of pH is an important consideration in flume studies involving silt.

A graph of specific gravity versus kinematic viscosity is presented in Figure 4 to give some feeling for the wide range of kinematic viscosity attainable using sucrose. This range is desirable as it allows for a continuous spectrum of scale ratios by simply adding more sucrose to the solution or diluting the solution thus decreasing the viscosity.

Procedure

In order to ensure the validity of the data gained in these experiments it was necessary to make three runs proving the effectiveness of the Reynolds-Froude scale modeling technique. Several studies have proven its effectiveness in sedimentology in scaled-down models (Southard & Boguchwal & Romea 1980, Boguchwal, 1977) in which scaled-down models are used to simulate larger features, but no data exist to prove the validity of scaled-up models, those which simulate smaller features on a larger scale.

Runs 1, 2, and 6 were responsible for testing scaled-up models using Reynolds-Froude modeling. In Run 1 the 115 μm sand was used in a sucrose solution of kinematic viscosity 8 cS giving a scale ratio of 4, thus sediment of mean size 28.8 μm. In Run 2, the 20.5 μm silt was used in water

which, due to the temperature, had a kinematic viscosity of 0.60 CS thus a scale ratio of 1.4 and an effective silt size of 28.9 μm. Run 6 was an insurance run, using the sand in water at approximately the same flow depth and mean flow velocity as Run 1 to prove that the large ripples in Run 1 were due to viscosity differences, not to differences in grain size, flow depth, or mean flow velocity.

Runs 3, 4, and 5 consisted of a fairly long run using the silt, with each run having a different sucrose concentration in the solution, thus a different kinematic viscosity. The scale ratios obtained were 2, 3, and 4.8 respectively.

The basic procedure was the same for all six runs. In each run the ripples were allowed to come to equilibrium over a period of time averaging about 24 hours. An equilibrium condition was one in which ripple shape, migration rate, and suspended-sediment concentration were approximately constant along the bed during the migration of at least a few ripples. A time-lapse 16 mm camera began filming when the bed was judged to be in equilibrium, and 35 mm pictures were taken throughout the run. Measurements obtained from the 16 mm film included flow depth, ripple height and spacing, lee-side angles, and migration rate. Each run contained at least one five-hour segment (except for Run 6, 2.5 hours) during which 20 ml samples of suspended and total sediment concentrations were drawn every 15 minutes from which hourly averages were determined. An average water-surface slope was obtained by taking

measurements with a point gauge along the the centerline of the flume over a 5 m section. Each run with silt was limited somewhat due to the life of the mechanical seal within the pump. Silt grains are capable of getting into the seal and wearing it down rapidly. In order to ensure that the necessary runs were made, it was necessary to limit the length of the runs and this unfortunately also limited the amount of data taken.

REYNOLDS-FROUDE SCALE MODELING IN SEDIMENTOLOGY

DYNAMIC AND GEOMETRIC SIMILITUDE

Dimensional analysis is a method which allows one to examine a particular problem in detail without having to know the equations governing the particular problem. Instead one need only know the variables involved in the problem. By knowing the complete set of variables which characterize a system one can rearrange this set into a smaller, more workable group of dimensionless variables which allow for a dynamic and geometric one-to-one correspondence between the two systems. The important theorem in dimensional analysis first given by Buckingham (1914) states that given a set of n original variables which characterize a particular problem, the number of dimensionless groupings of the original variables needed to completely specify the problem is N - m, where m is the number of dimensions in the problem, usually mass, length and time. Dimensional analysis has been used for many years in engineering problems but has only recently been applied for scale modeling purposes in geology (Southard and Boguchwal, 1980; Boguchwal, 1977).

IMPORTANT VARIABLES

If one were to think of variables present in a flume study, a rather substantial list would result. Since the

aim of dimensional analysis is to limit the list of variables while still effectively characterizing the system, some variables of secondary importance may be eliminated. Some good initial assumptions would include steady, uniform flow in a straight, open, and very wide channel of constant depth. A possible set of variables might then include the sediment characteristics of grain shape, mean size, packing, and sorting; fluid properties of density and viscosity; flow properties of depth and velocity or shear stress and environment properties of bottom slope and gravity.

By making the further key assumptions that sediment sorting, packing and shape, and bottom slope are of secondary importance, the list is reduced to seven variables (Fig. 6):

p_s : sediment density
D : mean sediment size
p_f : fluid density
μ : fluid viscosity
d : mean flow depth
U : mean flow velocity or
T : shear stress
g : gravity

Since a given value of shear stress can specify more than one bed state, mean flow velocity is preferable to shear stress in characterizing the flow.

Using Buckingham's theorem, this list is reduced to four dimensionless variables, with an appropriate group being a density ratio, a Reynolds number, a Froude number,

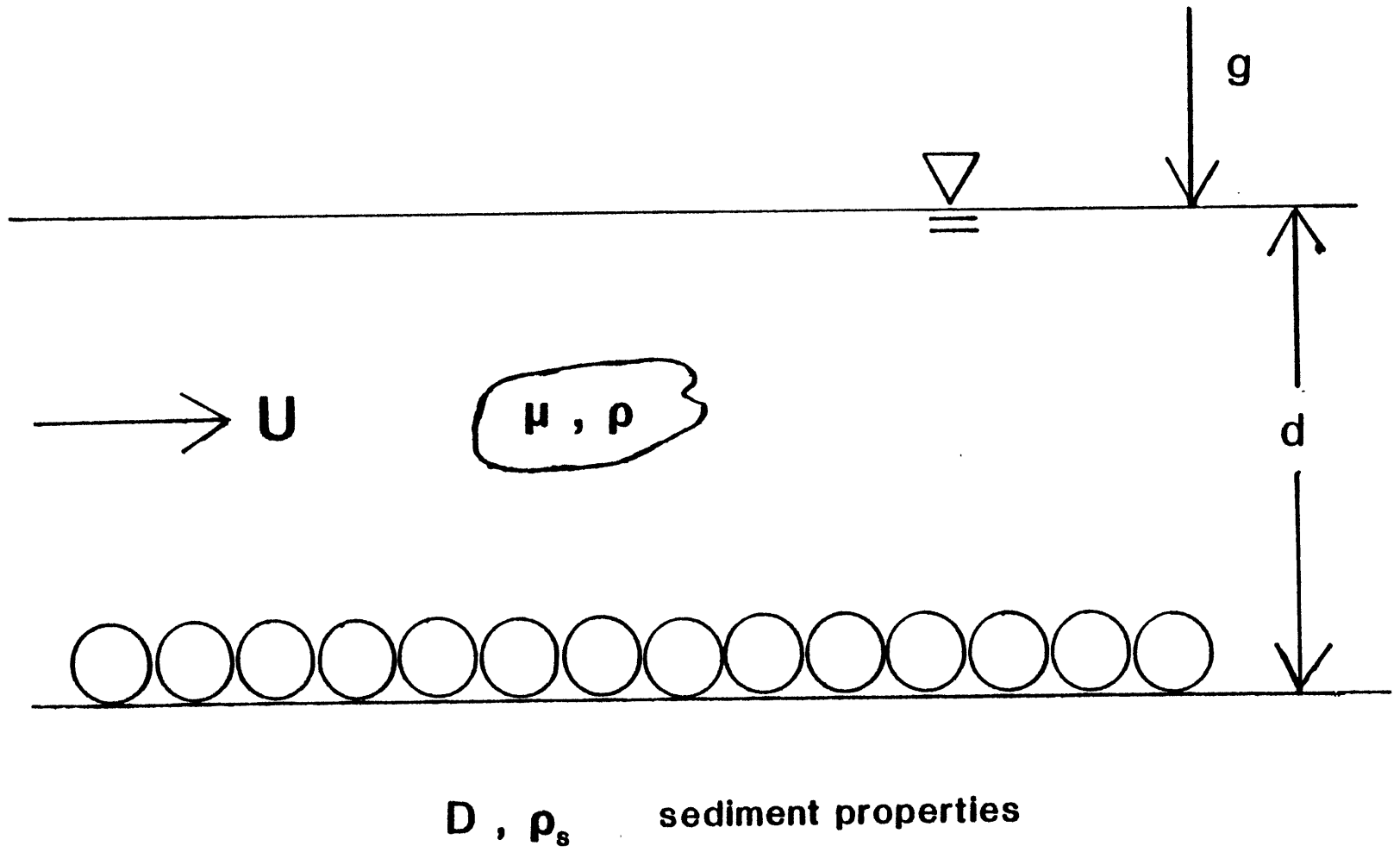

FIGURE 6: Set of fundamental variables used in Reynolds-Froude Modeling technique.

and a size ratio:

$$p_s/p_f \qquad pUd/\mu \qquad U/(gd)^{1/2} \qquad d/D$$

For dynamic and geometric similitude between two flows, each dimensionless ratio must be equivalent in both the original and the model flow. Since g is effectively invariables, model flow velocity is fixed by equality of Froude numbers:

$$U_r = (d_r)^{1/2}$$

where the subscript r refers to the ratio between the original and the model flow. It is then possible to fix viscosity by equality of Reynolds numbers or:

$$\mu_r = p_r(d_r)^{3/2}$$

or in terms of kinematic viscosity, $\nu = \mu/p$

$$\nu_r = (d_r)^{3/2} \quad .$$

Using dimensional analysis, maximum scale ratios can be achieved by choosing fluids of appproximately equivalent densities but with widely different viscosities. From a previous study which used Reynolds-Froude modeling (Southard et al., 1980) correctness of modeling exists if the frequency distributions of the geometric properties of height and spacing and the dynamic property of ripple migration rate scale properly.

Scaled-up modeling is important in research where it is necessary to observe small-scale features such as initiation of grain movement of formation of ripple laminae. Fluids such as water-sucrose of water-glycerol solutions have approximately equivalent densities to that of water

with widely different viscosities, thus allowing for large scale ratios. It is important to remember that all factors scale in Reynolds-Froude modeling, thus just as grain size can be scaled by a factor of five, so too will flume geometry and flow depth. Thus one should exercise some control over scale model size ratio so that one does not create scales of such size that their relevance to natural situations becomes questionable.

RESULTS

DATA PRESENTATION

Detailed measurements of each ripple in all six runs are presented in tabular form in Appendix 2. These measurements have not been scaled and represent what was actually seen in the films. Table 2 is a summary of most of the measured and derived variables obtained from the six runs. Data presented are unscaled. The values of water-surface slope and bed shear stress were corrected for the small width-to-depth ratios in the flume using the correction factor of Williams (1970). This was necessary as the appropriate width-to-depth ratios in flumes should exceed 7 but the values in this study were only 1.2 to 3.2. Tables 3 and 4 present scaled values for some of the more important measured and derived variables in the study.

Since all data collected in these runs were obtained by viewing the ripples through the Plexiglas observation area, some comments should be made concerning the validity of extrapolating ripple morphology seen through the sidewalls to that actually present in the channel. Upon draining the fluid from the flume, ripple crests were observed to be straight crested across the entire width of the flume. One noticeable difference was that ripple crests met the troughs at sharper angles along the center of the flume than at the flume sidewalls. Otherwise the

TABLE 2

Experimental Data for Runs 1-6

	Run 1	Run 2	Run 3	Run 4	Run 5	Run 6
Measured Variables						
Duration, hours	11:20	7:40	5:15	8:10	8:40	3:25
Discharge, q l/s	10.3	3.3	3.7	6.1	6.0	11.4
Depth, d cm	11.2	4.7	4.8	7.3	7.6	12.7
Temperature, t°C	34.4	45.0	42.3	45.0	44.4	41.7
Water Surface Slope, S	0.004	0.0043	0.0038	0.0029	0.0032	0.0023
Suspended Sediment Concentration, Css gm/l	26.7	18.7	15.6	20.1	24.0	18.3
Total Sediment Concentration Ct gm/l	27.3	19.9	15.8	20.2	26.2	18.9
Ripple Spacing (cm)	53.3	9.2	18.1	27.8	44.6	12.4
Ripple Height, H cm	5.10	0.80	1.42	1.23	1.50	1.55
Flume Width, W cm	15.0					
Specific Gravity	1.207		1.136	1.180	1.221	
Hours to Equilibrium, hours	24:30	26:45	30:00	21:00	30:30	5:20
Derived Variables						
Mean Velocity, U cm/s	61.3	46.8	52.9	56.1	52.7	59.7
Bed Shear Stress, τ dynes/cm^2	0.056	0.020	0.021	0.025	0.030	0.029
Froude Number, Fr	0.59	0.69	0.77	0.66	0.61	0.54
Reynolds Number, Re	8582	36660	8464	7875	3814	120348
Suspended Sediment Transport Qss gm/cm-s	1.64	0.88	0.83	1.13	1.26	1.09
Total Sediment Transport Qt gm/cm-s	1.67	0.93	0.84	1.13	1.38	1.13
Bed Load Transport, Qb gm/cm-s	0.07	0.03	0.10	0.09	0.13	0.48
Kinematic Viscosity, ν cS	8.0	0.60	3.0	5.2	10.5	0.63
Fluid Density, p_f gm/cm^3	1.204	0.990	1.131	1.176	1.220	0.992

ripple morphology was constant across the channel. It is suspected that flume sidewall effects would be more significant for high-velocity three-dimensional ripples.

TEST RUNS

In order to effectively test the Reynolds-Froude modeling technique it was necessary to effectively scale mean grain size for the sand and silt. Sand in Run 1 was scaled by a factor of 4 to allow for an effective sediment size of 28.8 microns (Table 3). The silt was scaled by a factor of 1.4 to an effective size of 28.9 due to decreased kinematic viscosity as the pump heated water to a temperature of 34.4° (CRC Handbook of Chemistry and Physics). Curves were constructed for the scaled silt and sand (Fig. 7) displaying the similar effective mean values and sorting characteristics of the sediments.

Effectiveness of the modeling technique was evidenced by the closeness of mean ripple spacings, 13.3 cm and 12.9 cm, mean ripple heights, 1.28 cm and 1.12 cm, and mean ripple migration rates, 0.48 and 0.31 cm/min, for the scaled sand and silt, respectively. Figures 8, 9, and 10 present frequency curves for the scaled silt and sand runs which further stress the closeness of the scaled runs relative to Run 1 unscaled.

In order to dispel any possible doubts that the large ripples in Run 1 were due to anything other than fluid viscosity differences, Run 6 was performed. In it the

TABLE 3

Scaled Data: Runs 1-6

Run #	U cm/s	D μm	d cm	$\bar{L}$ cm	$\bar{H}$ cm	Migration Rate cm/min
1	30.7	28.8	2.8	13.3	1.28	0.48
2	55.4	28.9	6.6	12.9	1.12	0.31
3	37.4	10.3	2.4	9.1	0.71	0.06
4	32.4	6.8	2.4	9.3	0.41	0.10
5	24.1	4.3	1.6	9.3	0.31	0.03
6	69.6	156.0	17.3	16.9	2.11	2.36

FIGURE 7: Cumulative percent curves for the scaled sand and the scaled silt.

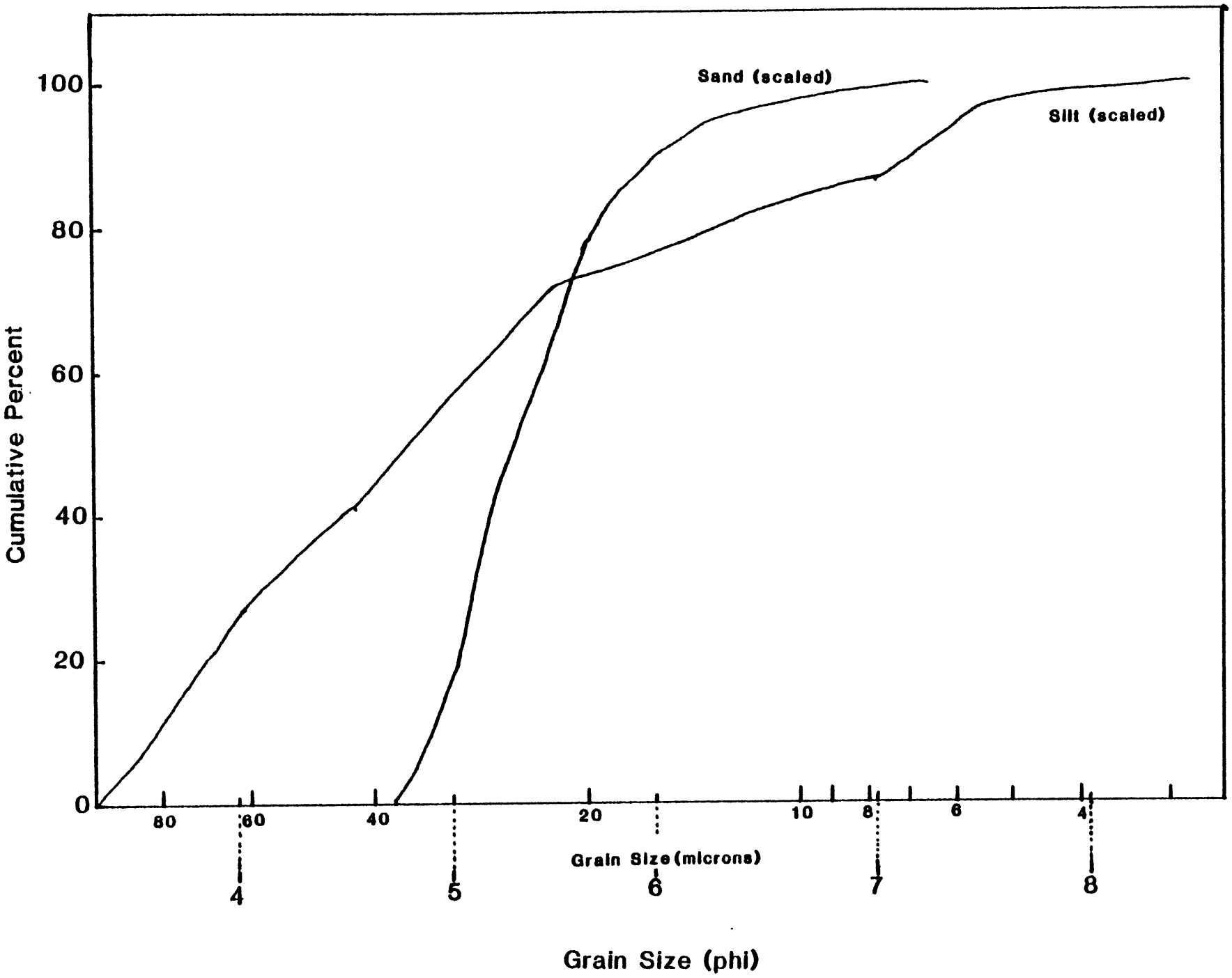
Sand (scaled)
Silt (scaled)
Cumulative Percent
100
80
60
40
20
0
80
60
40
20
10
8
6
4
Grain Size (microns)
4
5
6
7
8
Grain Size (phi)

FIGURE 8: Frequency vs spacing curves for the test runs. Note the difference between Run 1 unscaled and Run 1 scaled.

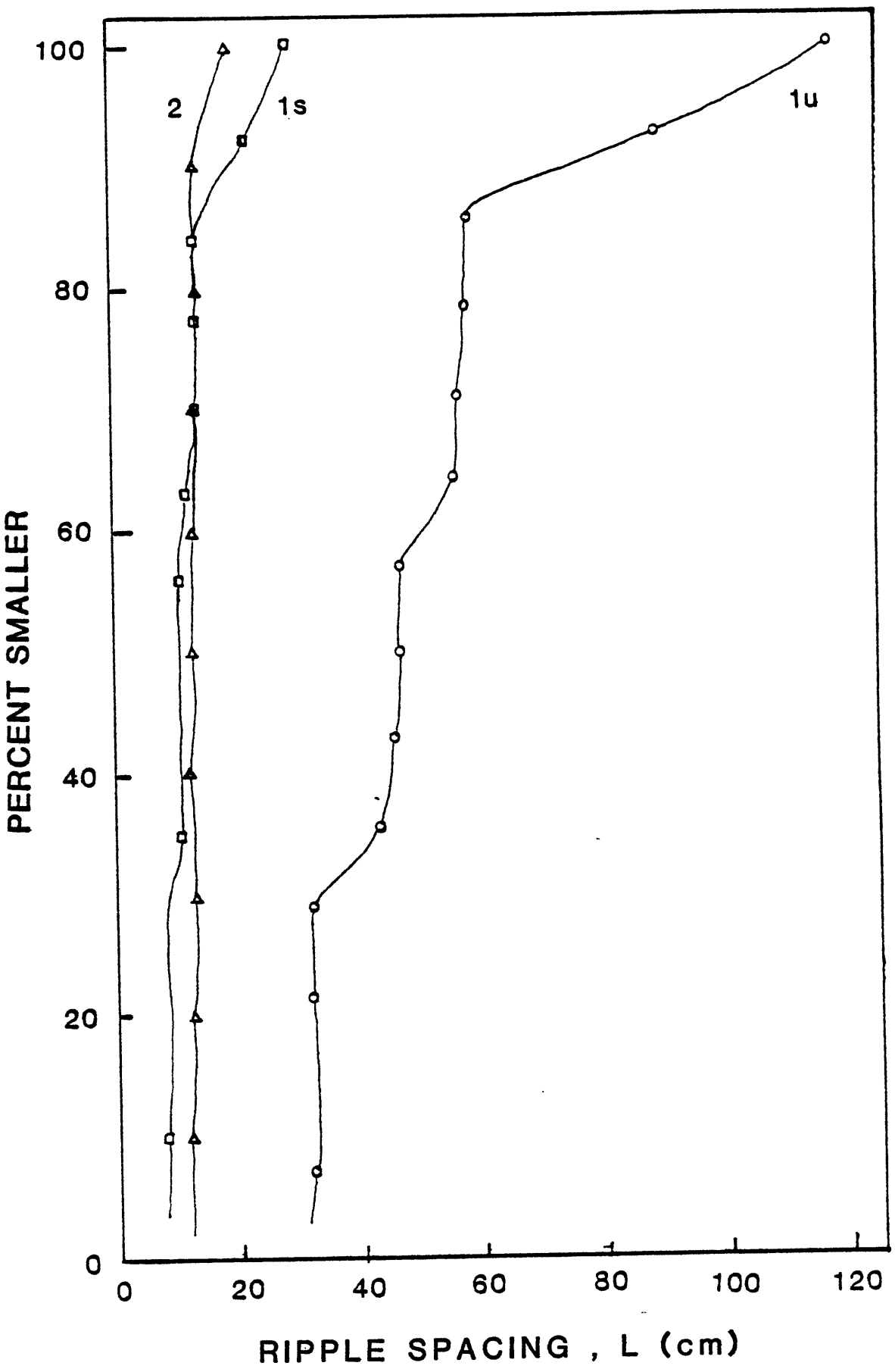
100
80
60
40
20
0
PERCENT SMALLER
2
1s
1u
0
20
40
60
80
100
120
RIPPLE SPACING , L (cm)

FIGURE 9: Frequency vs height curves for Runs 1 and 2. Note the good agreement between Run 1 scaled and Run 2.

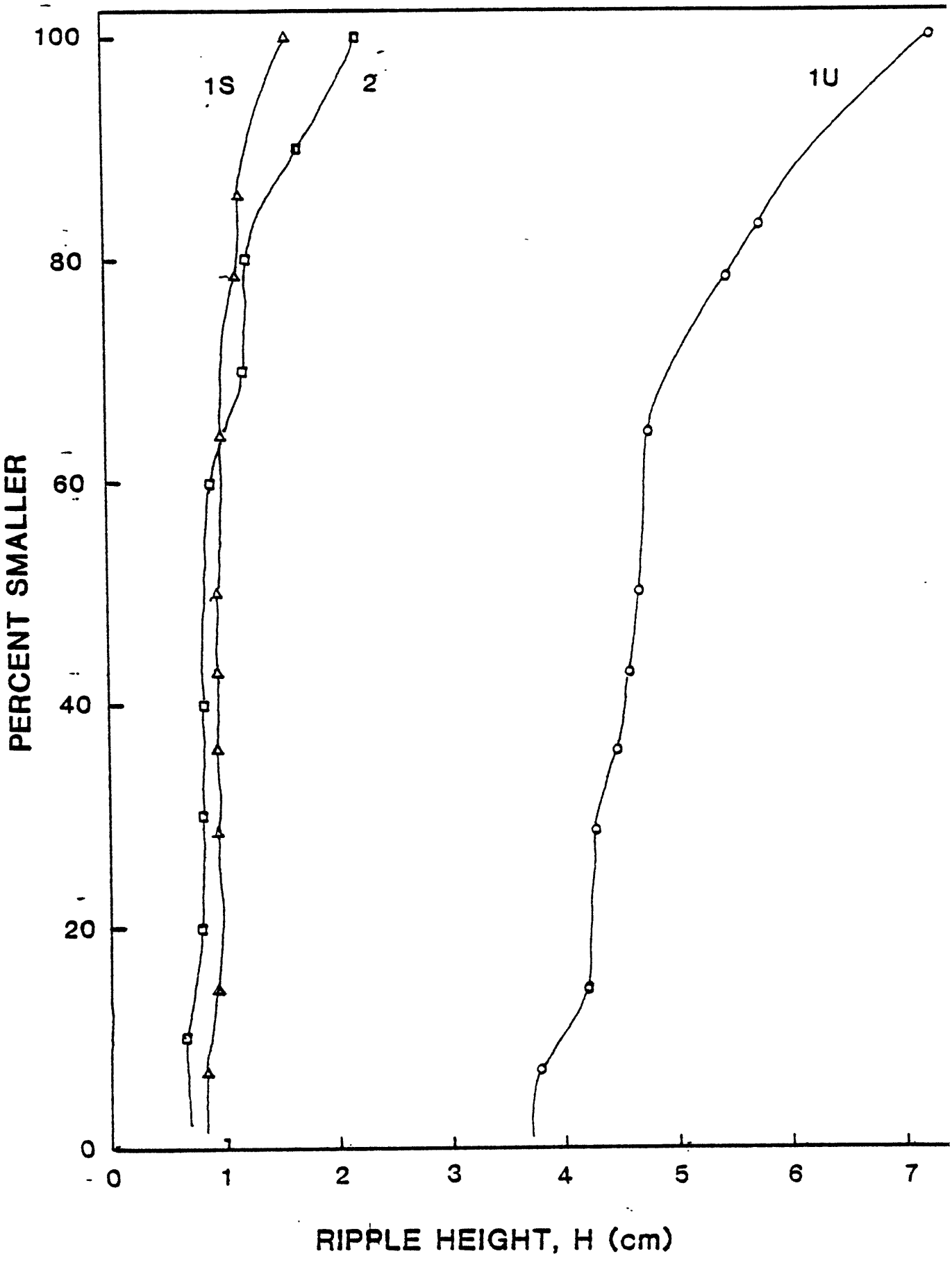
100
80
60
40
20
0
PERCENT SMALLER
1S
2
1U
0
1
2
3
4
5
6
7
RIPPLE HEIGHT, H (cm)

FIGURE 10: Frequency vs migration rate curves for Runs 1 and 2.

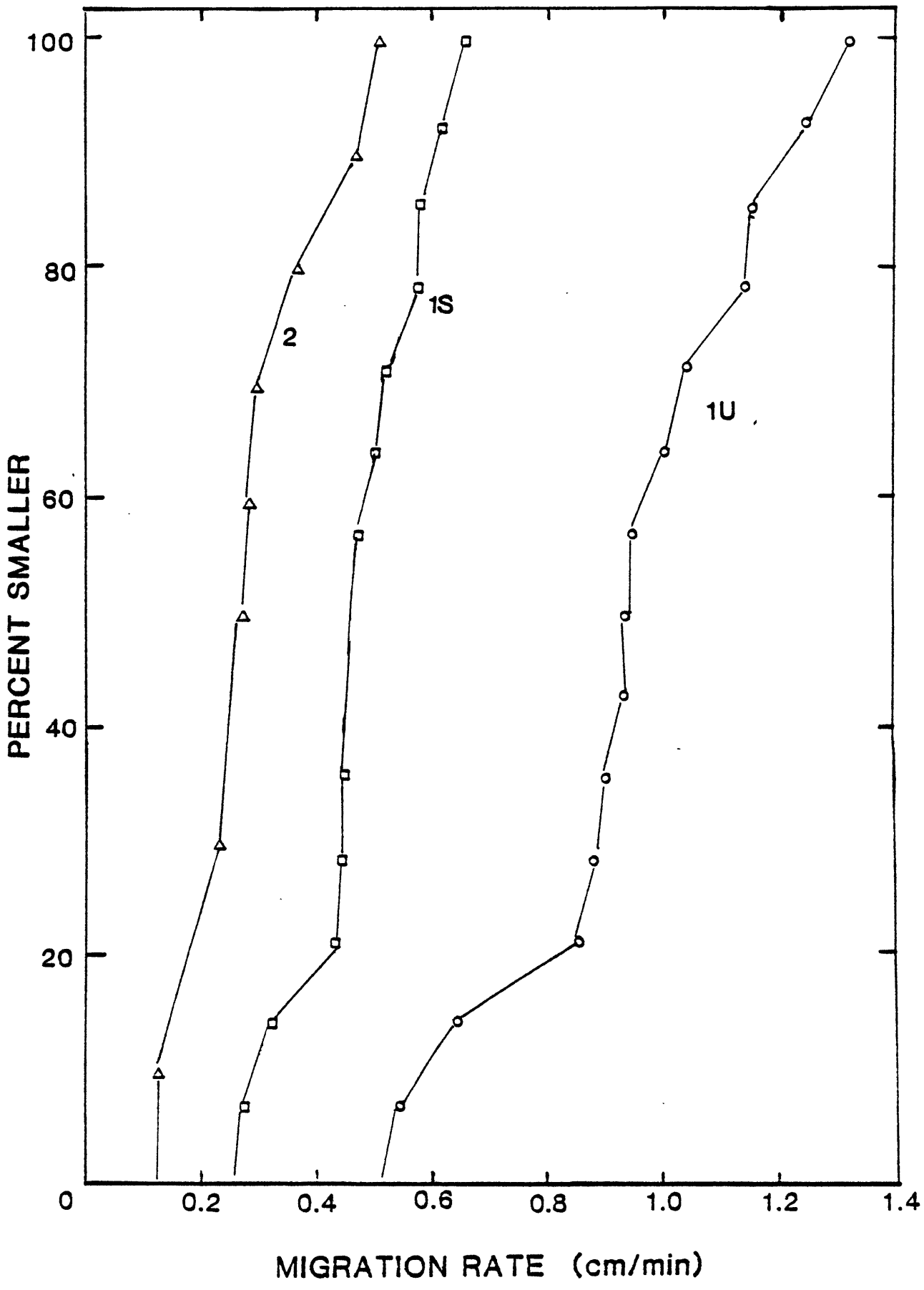
100
80
60
40
20
0
PERCENT SMALLER
0.2
0.4
0.6
0.8
1.0
1.2
1.4
MIGRATION RATE (cm/min)
2
1S
1U

measured variables of mean flow depth and mean flow velocity were set so as to agree with the unscaled values of Run 1. The only difference between the two runs was due to fluid differences. From the data in Table 2 and Figures 11, 12, 13 it is obvious that significant differences between the two runs is due to viscosity differences between the flows.

Figures 14 through 18 are photographs of some typical ripples from Runs 1, 2 and 6. Note that the ripples morphology is similar in Runs 1 and 2. Ripples moved by slumping of grains at the brinkpoints of ripples in both runs. Suspended sediment transport rates were highest in Runs 1 and 2 and bed-load transport rate was lowest in these two runs. From Appendix 2, ripple indexes were similar for Runs 1 and 2: 10.3 and 12.7, respectively.

RUN 3

Photographs of typical ripples are presented in Figure 17 (photograph 14) and Figure 19. Average ripple spacing was 9.1 cm, height 0.71 cm, and ripple index was 12.8. Sclae ratio in Run 3 was approximately 2, giving an effective mean sediment size of 10.3 m (Table 3). Both height and spacing decreased somewhat from Run 2, with a drastic reduction in migration rate from 0.31 cm/min to 0.06 cm/min. Frequency curves for unscaled and scaled spacing, height, and migration rate for Runs 3, 4, and 5 are presented in Figures 20, 21, and 22, respectively.

FIGURE 11: Frequency vs spacing curves for Runs 1 and 6 unscaled. Note the lack of agreement between the two curves.

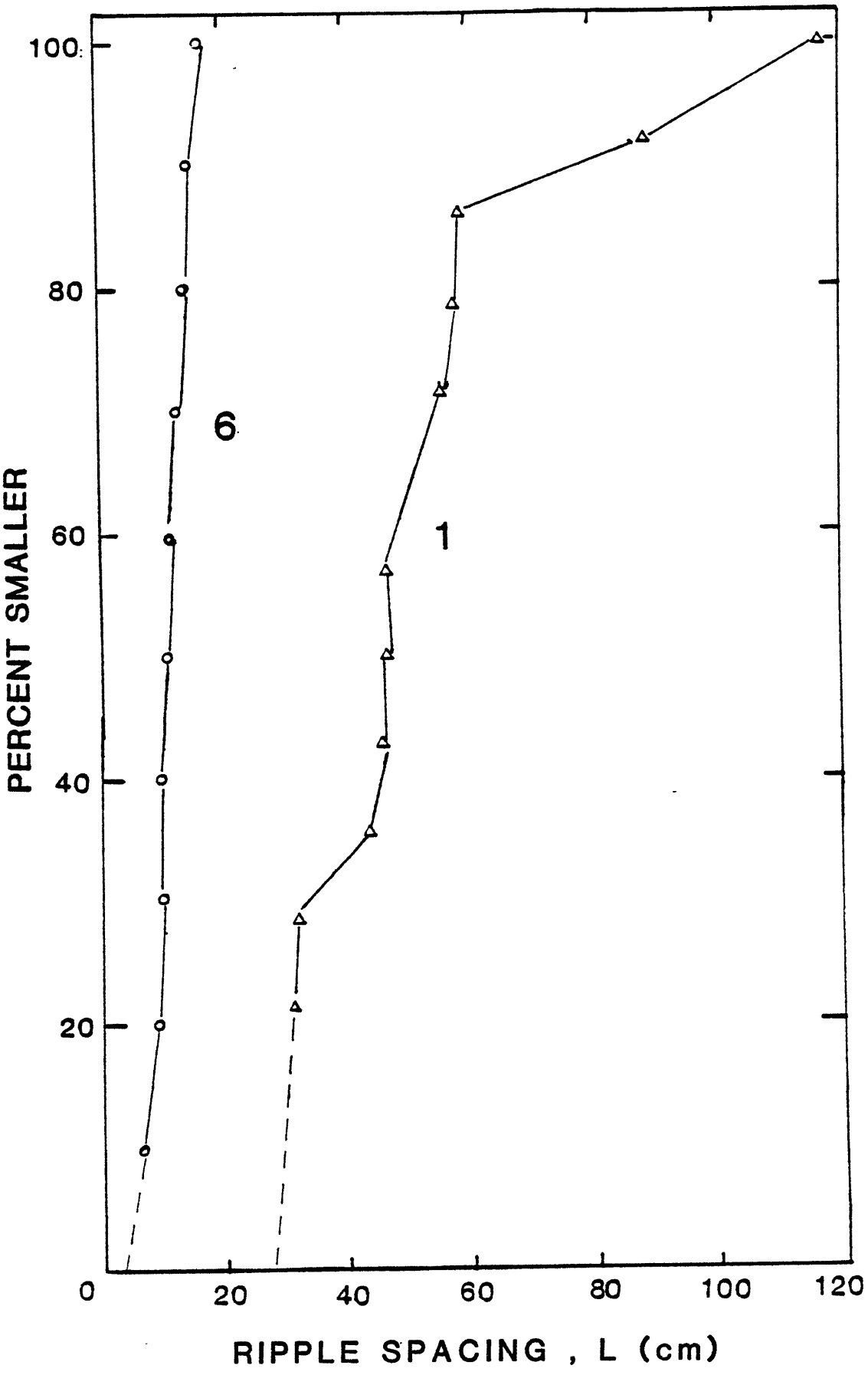
100
80
60
40
20
0
20
40
60
80
100
120
PERCENT SMALLER
RIPPLE SPACING , L (cm)
6
1

FIGURE 12: Frequency vs height curves for Runs 1 and 6. Note the wide differences between the two runs.

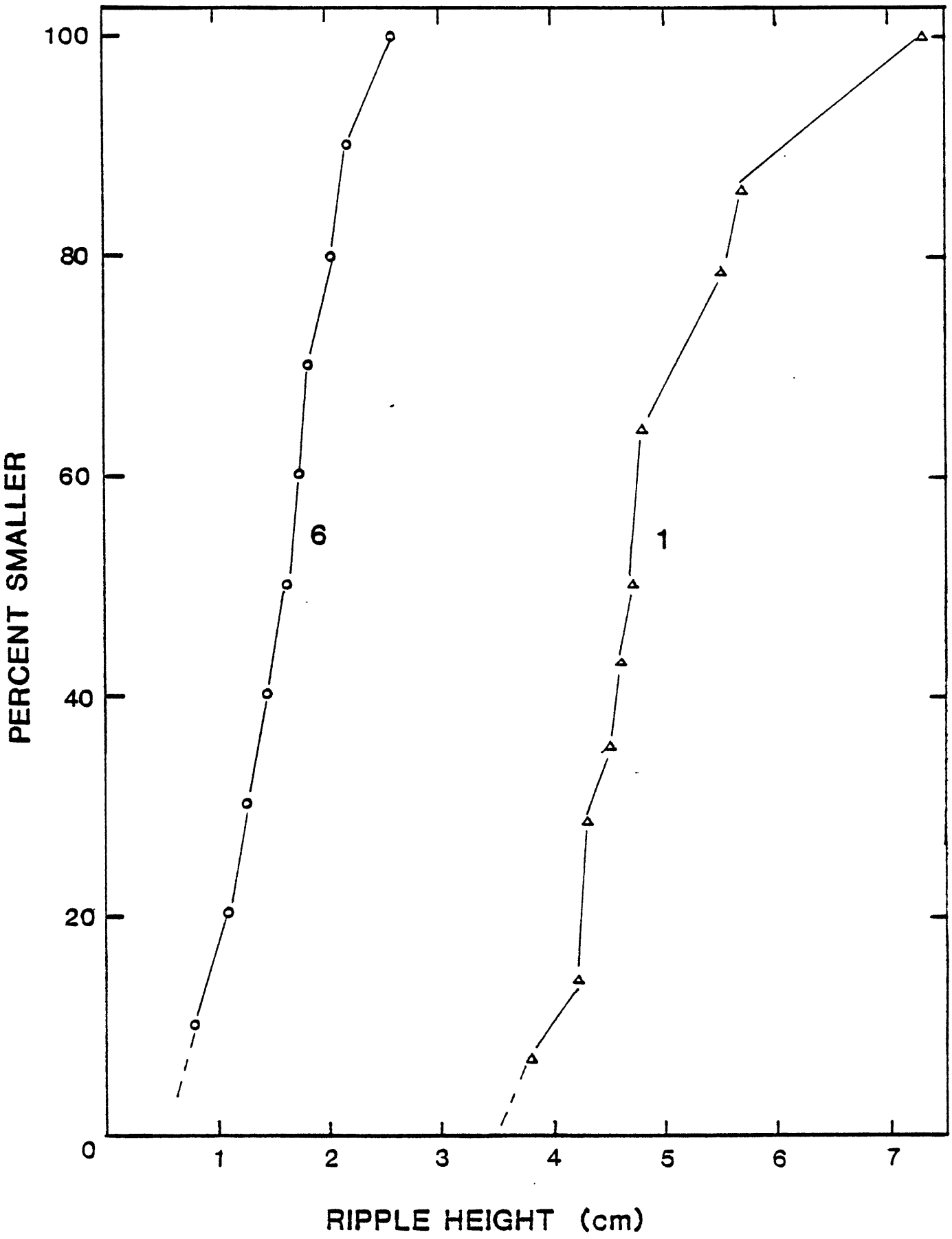
100
80
60
40
20
0
PERCENT SMALLER
6
1
1
2
3
4
5
6
7
RIPPLE HEIGHT (cm)

FIGURE 13: Frequency vs migration rate curves for Runs 1 and 6 unscaled. Note the lack of agreement between the two runs.

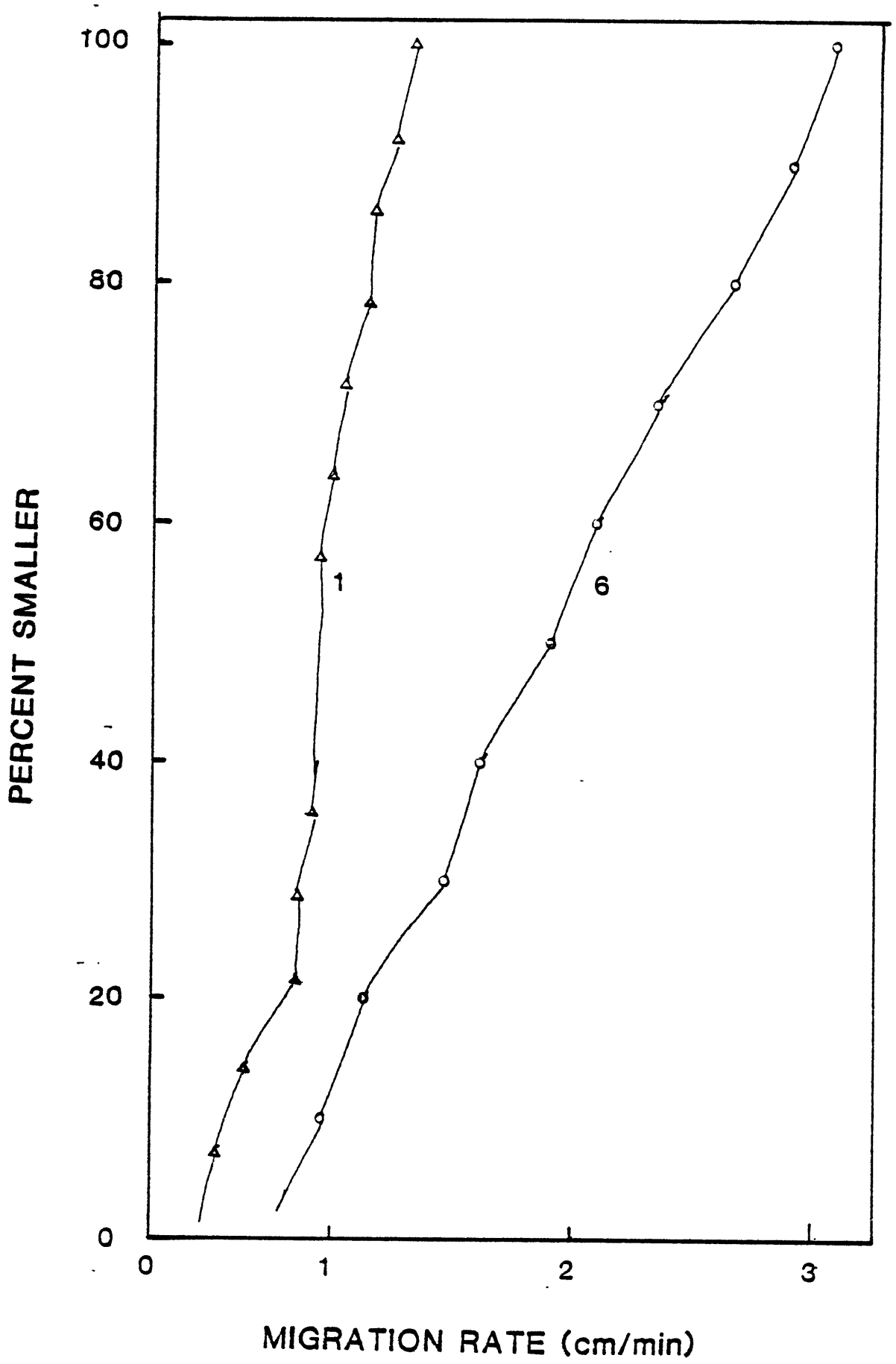
100
80
60
40
20
0
PERCENT SMALLER
0
1
2
3
MIGRATION RATE (cm/min)
1
6

FIGURE 14: Typical ripples from Run 1. The grid is a cm by cm grid. Note the steep slipfaces in both ripples as well as the stratification.

1

2

FIGURE 15: Some additional examples of ripples from Run 1. Note the stratification present in both ripples. The grid is a cm^2 grid.

3

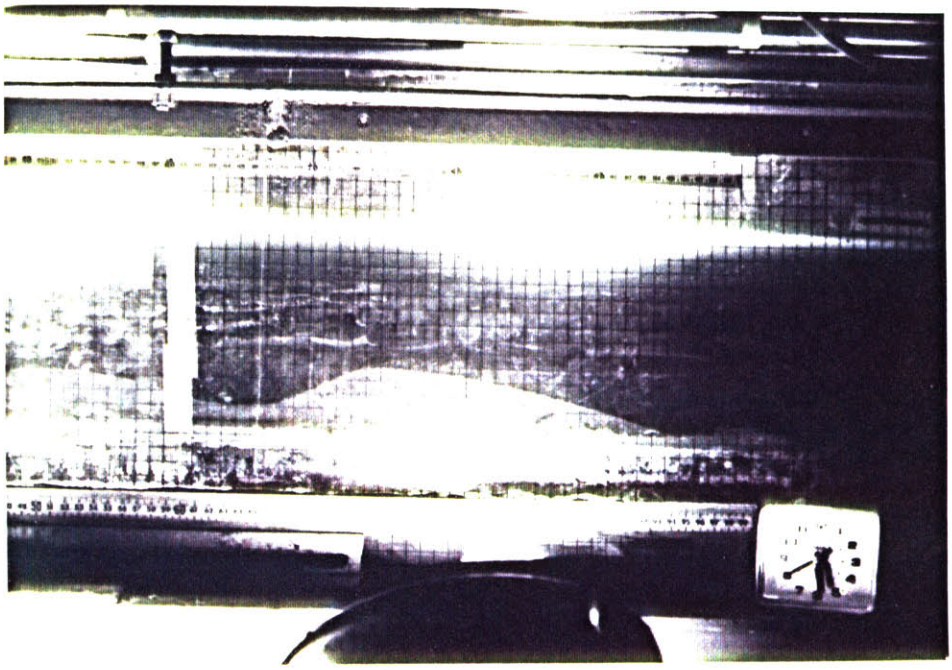

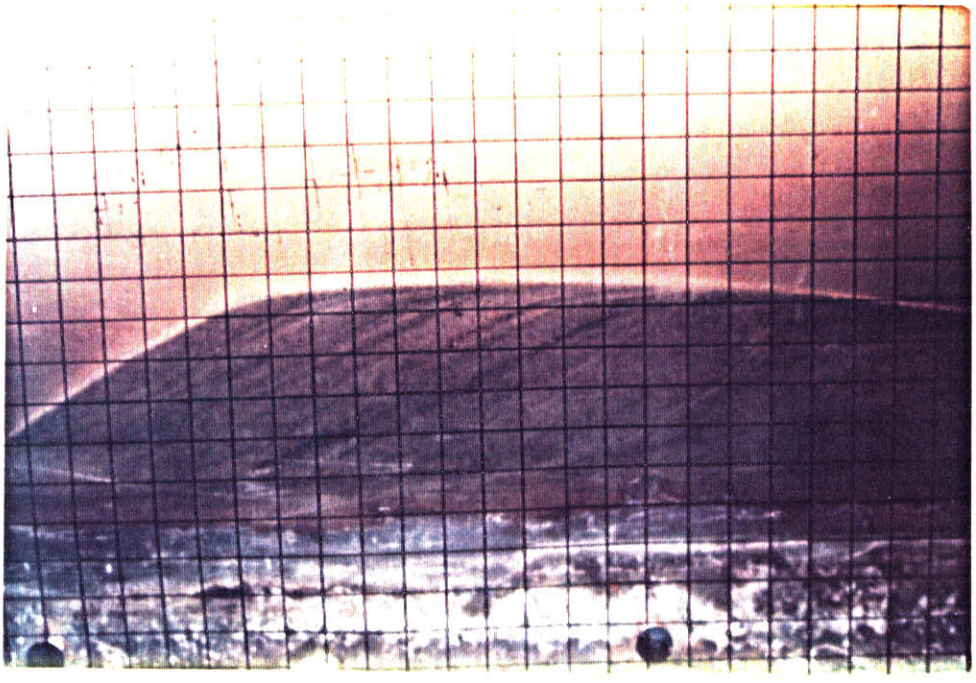

4

FIGURE 16: Some examples of stratification found in ripples from Run 2. Note the variability in ripple morphology between these ripples.

9

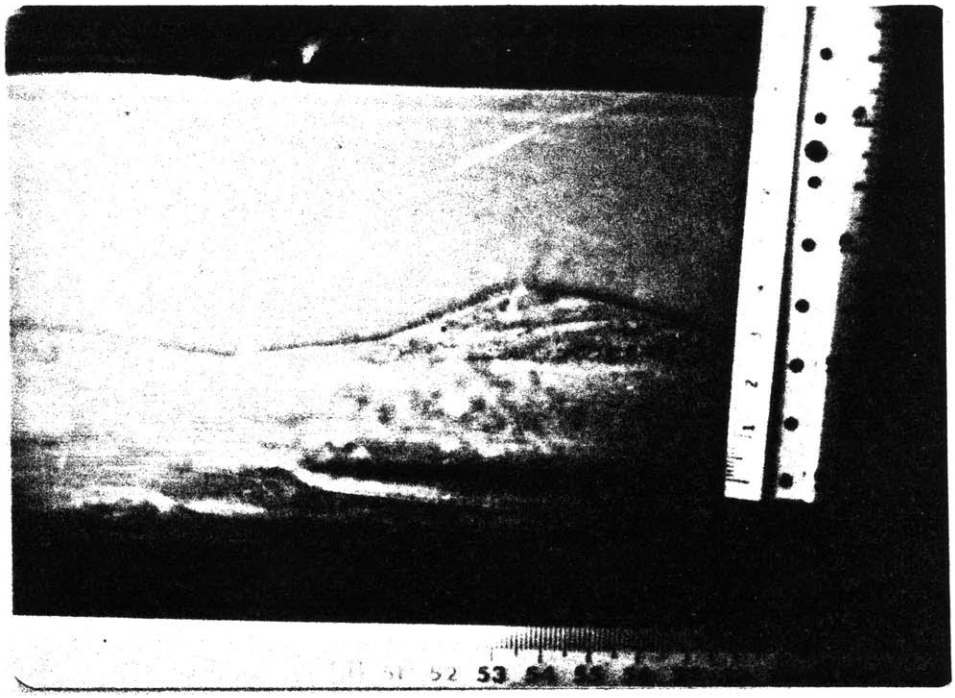

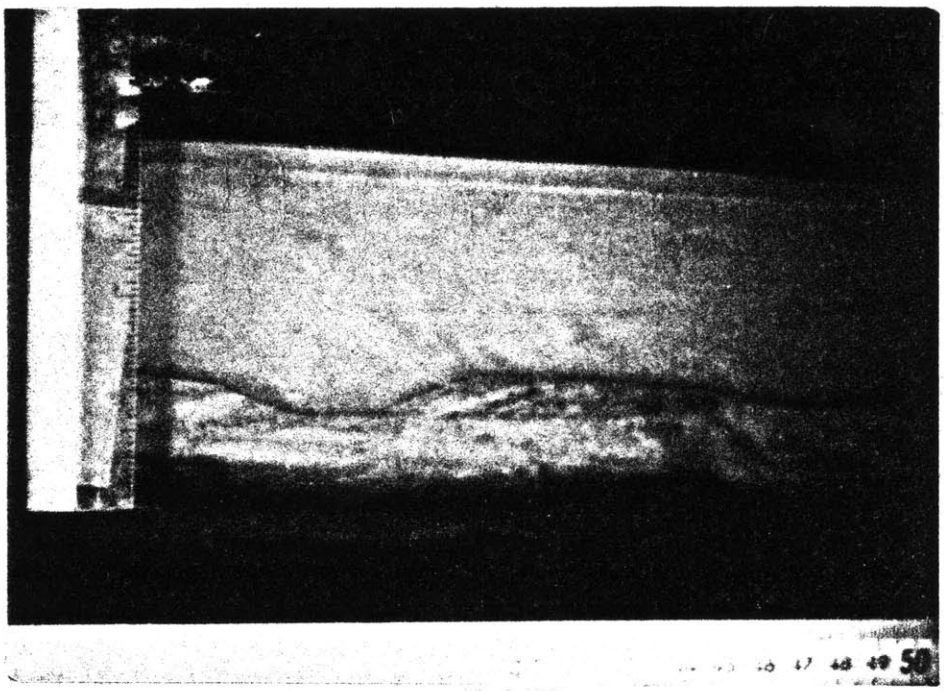

10

FIGURE 17: Photo 13 displays a ripple from Run 2, and photo 14 is from Run 4. Note that the spacings of these ripples differ greatly but the morphology and stratification are similar.

13

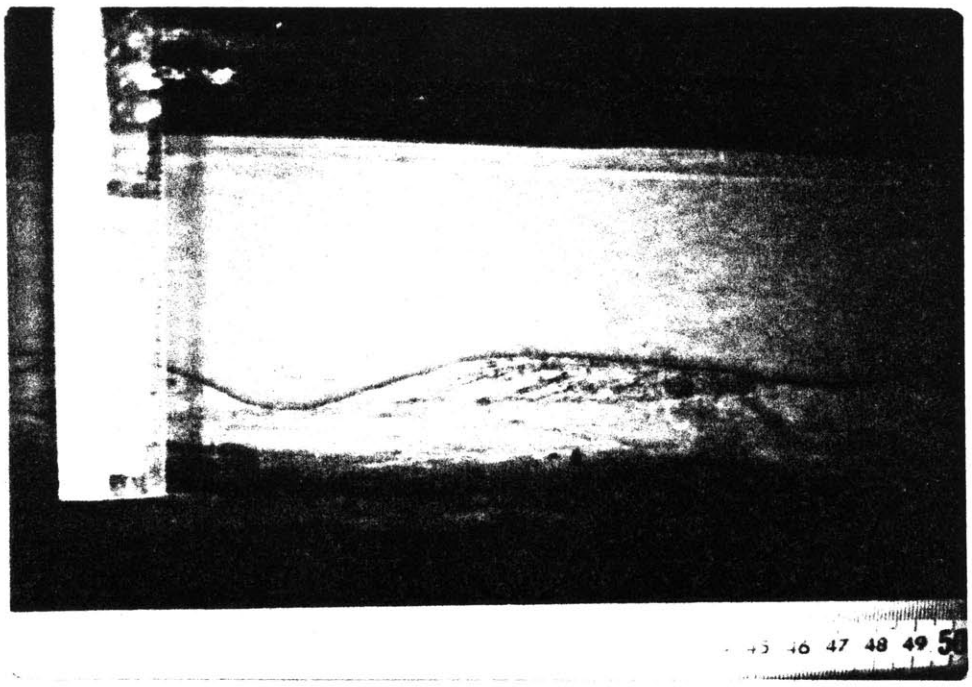

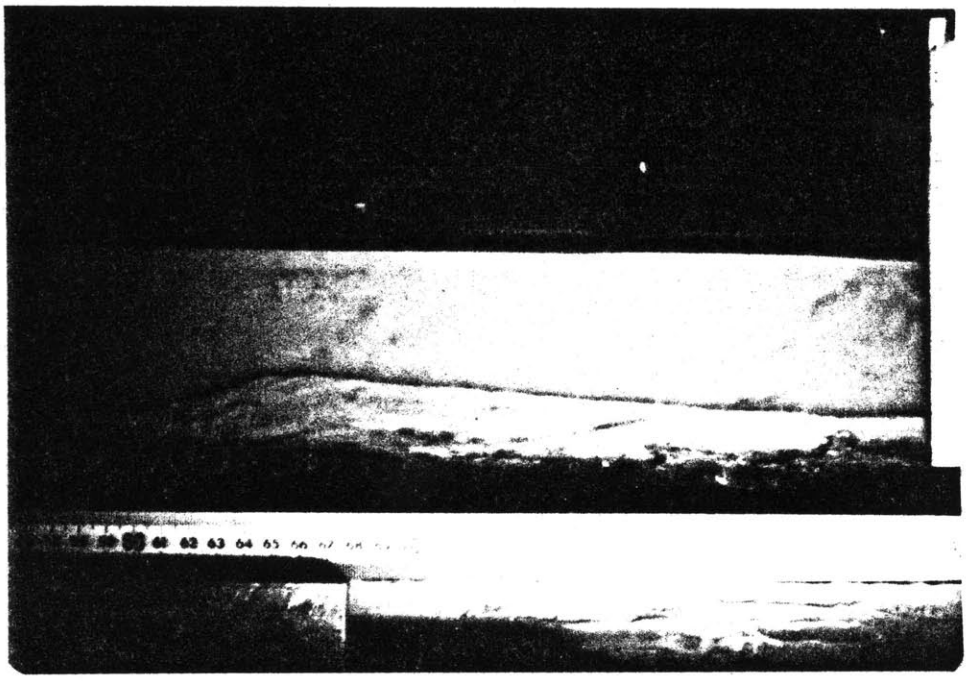

14

FIGURE 18: Some representative ripples from Run 6. Note the strong similarity in morphology in these ripples.

29

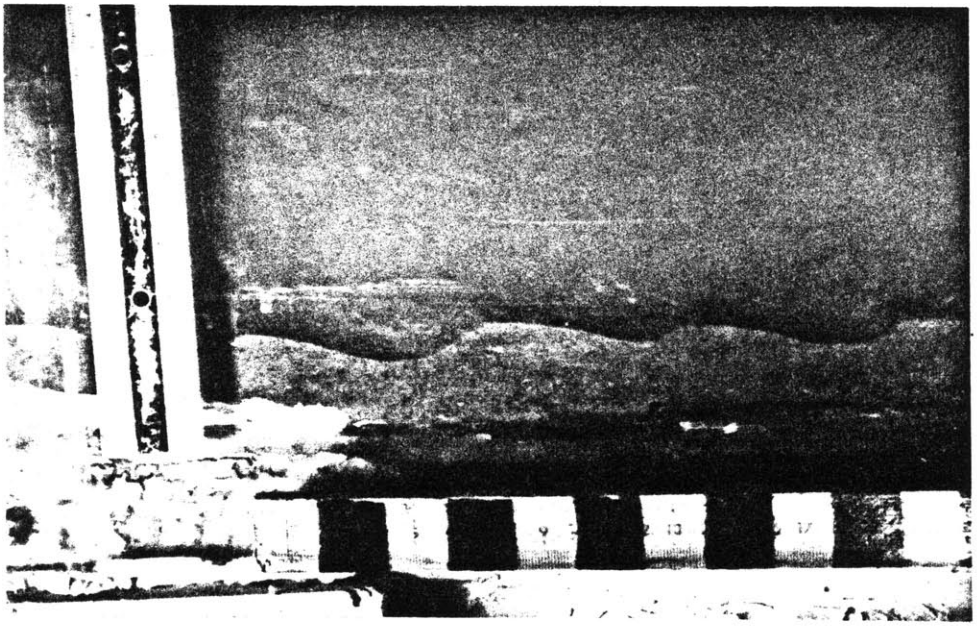

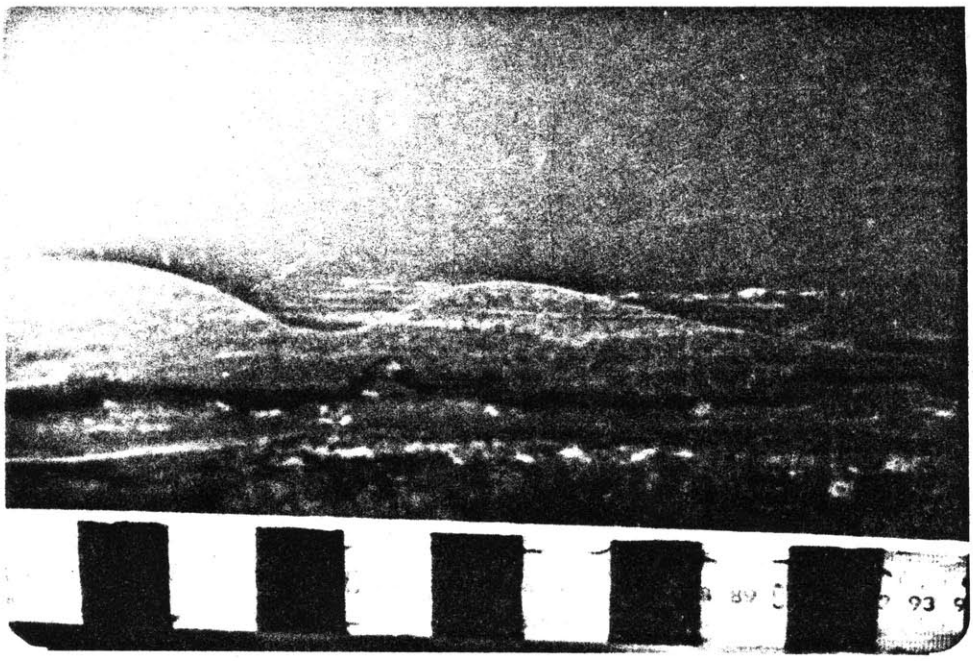

30

FIGURE 19: Examples of typical ripples from Run 3.

15

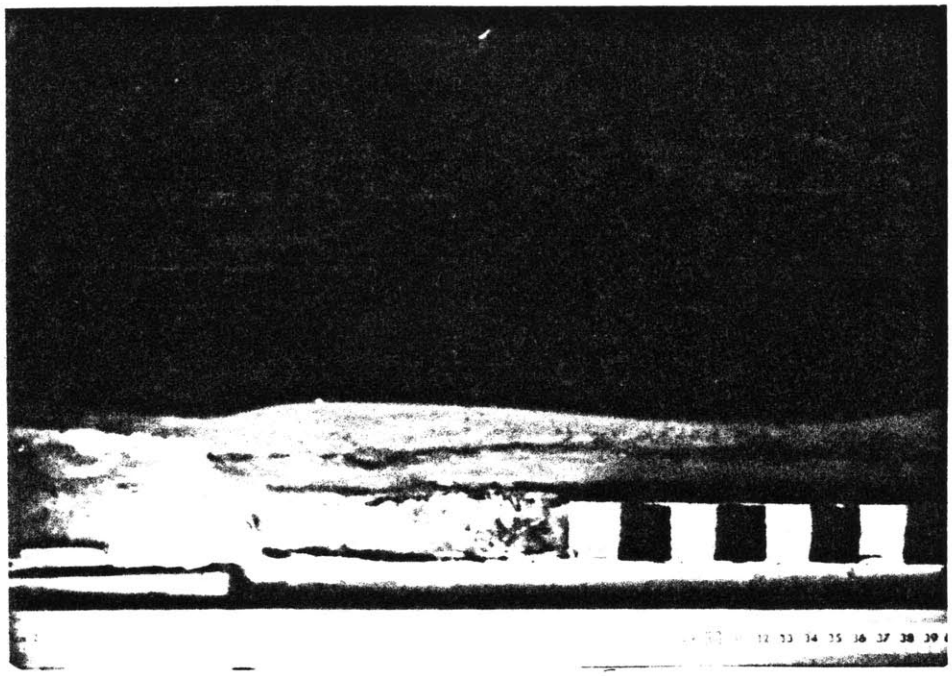

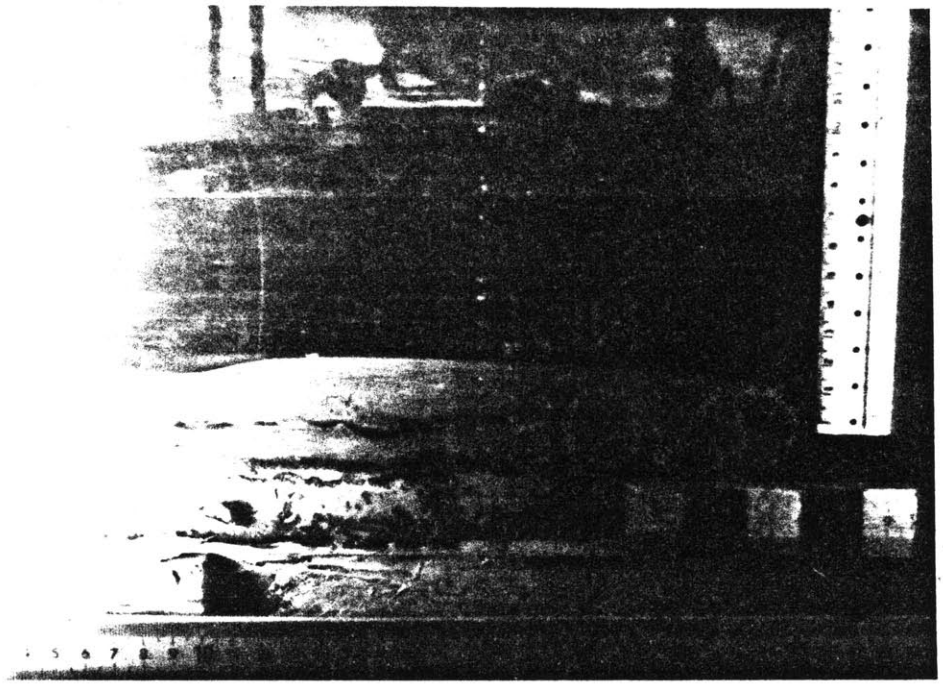

16

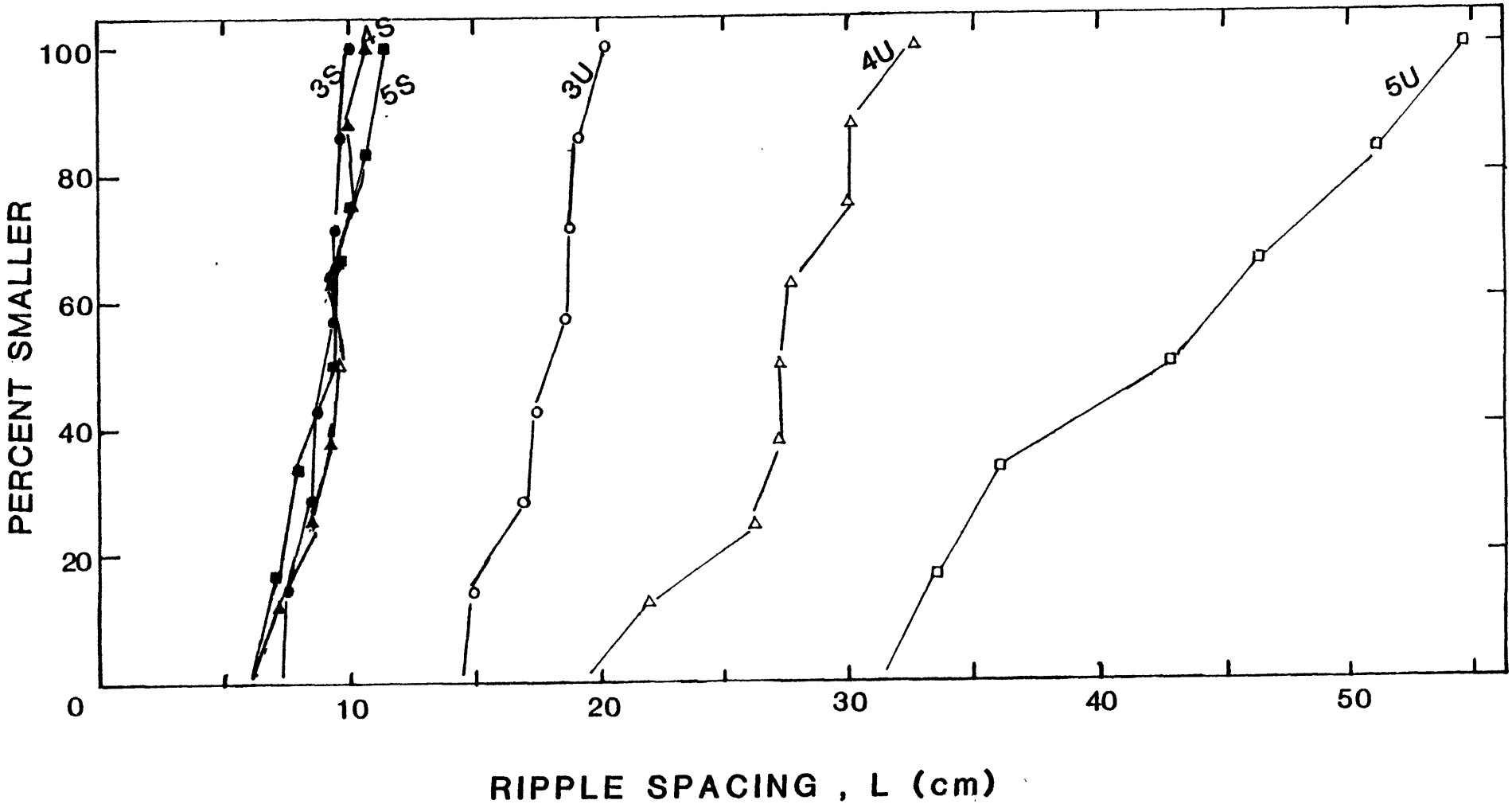

FIGURE 20: Frequency vs ripple spacing for scaled and unscaled Runs 3-5. Note the similarity in scaled spacing measurements.

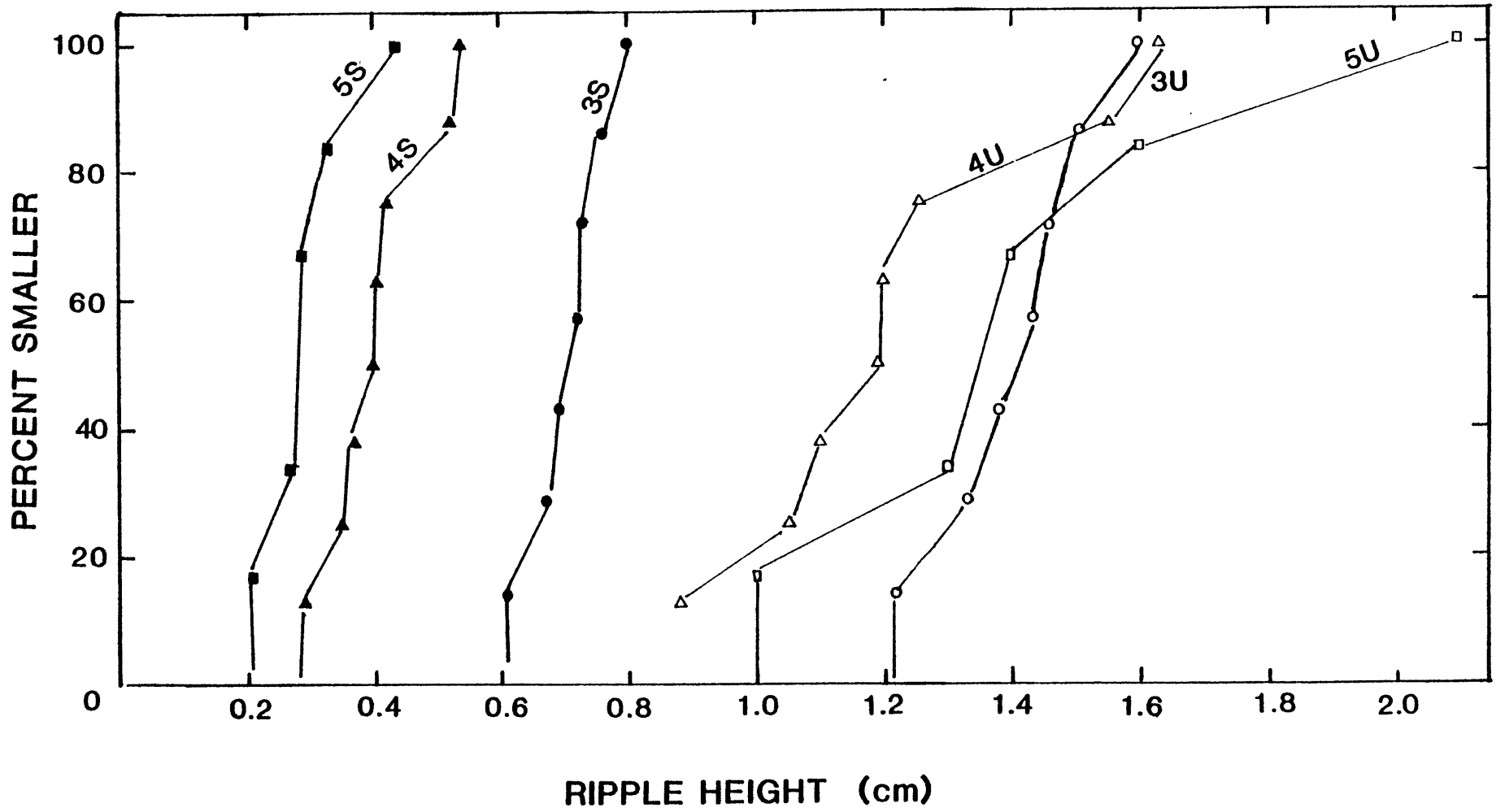

FIGURE 21: Frequency vs ripple heights for scaled and unscaled Runs 3-5. Note the steady decline in ripple heights with decreasing effective grain size in the scaled runs.

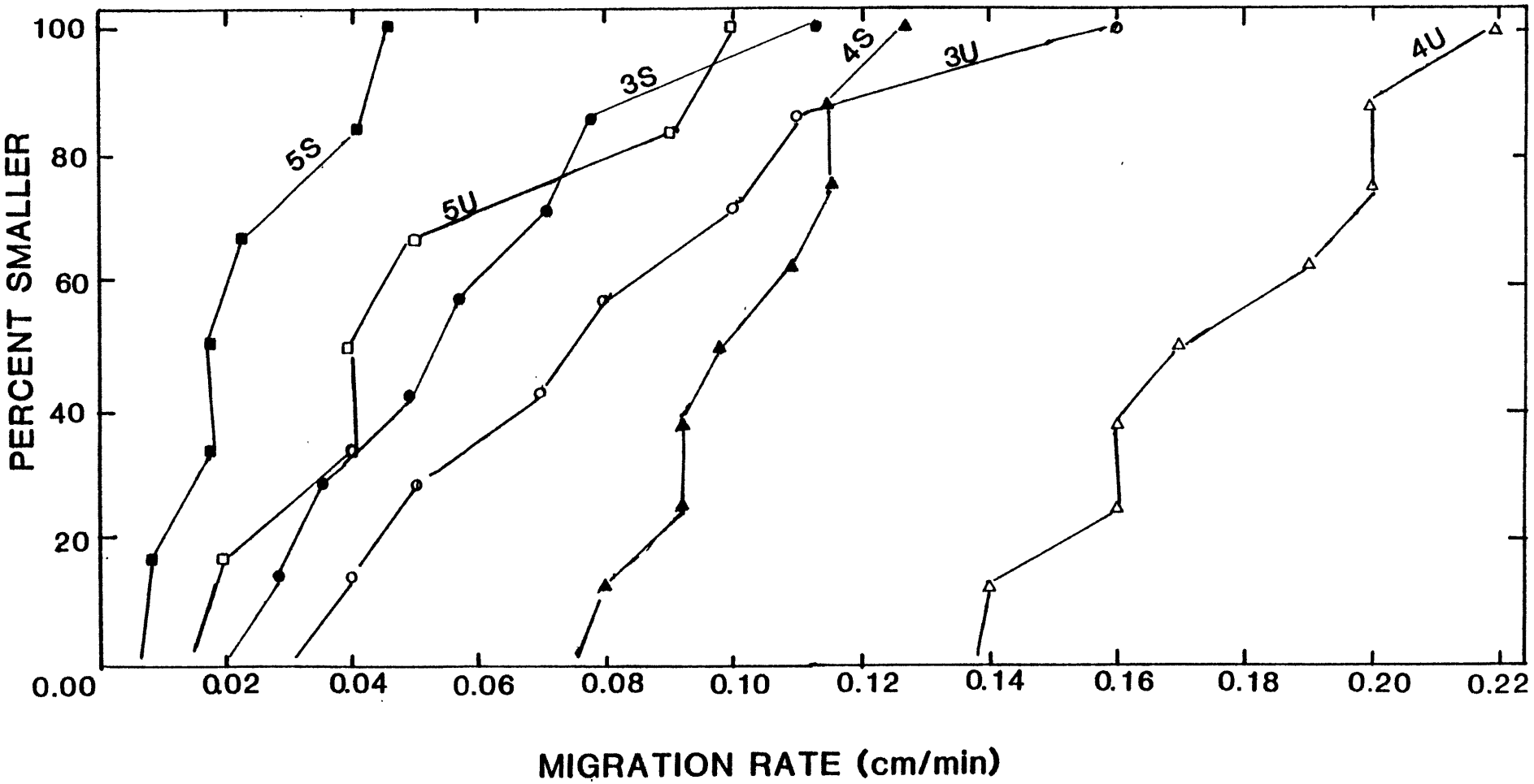

FIGURE 22: Frequency vs migration rates for scaled and unscaled Runs 3-5.

Sediment transport data, Table 4 indicates that almost six times as much sediment was transported in suspension as in bed load. Ripples moved as sediment crept up the stoss slope, piled up on the ripple crest, and avalanched down the lee slope. Sediment also accreted on the lee slope due to fallout from suspension. Mean slipface angle in Run 3 was approximately 22° (Appendix 2).

RUN 4

A scale ratio of 3 was obtained in Run 4, resulting in an effective grain size of 6.8 m and a mean flow velocity of 32.4 cm/s. Average ripple spacing and height were 9.3 and 0.41 cm, respectively, and migration rate was 0.10 cm/min. Ripple index for Run 4 was 22.9 (Appendix 2). Ratio of suspended to bed load transport was approximately 7, thus more sediment moved in suspension than in bed load. In this run ripple migration was due more to lee accretion of sediment through particle fallout than traction of sediment with successive avalanching of grains down the lee slope. Some typical ripples are shown in Figure 23. As in Run 3, the man value of the slipface angle was 22°.

Run 5

In Run 5 a maximum scale ratio of 4.8 allowed for an effective sediment size of 4.3 m and mean flow velocity of 24.1 cm/s. Figures 24.26 display the typical ripple morphologies seen in Run 5. Ripple heights were low and ripple index high, equalling 31.5. The mean

TABLE 4

Sediment Transport Data (scaled)

Run #	Css gm/l	Qss gm/cm-s	Ct gm/l	Qt gm/cm-s	Qb gm/cm-s	τ dynes/cm^2
1	26.7	0.82	27.3	0.84	0.07	0.014
2	18.7	1.04	19.9	1.10	0.03	0.028
3	15.6	0.57	15.8	0.59	0.10	0.010
4	20.1	0.65	20.2	0.65	0.09	0.008
5	24.0	0.57	26.2	0.63	0.13	0.006
6	18.3	1.27	18.9	1.32	0.48	0.039

FIGURE 23: Representative ripples from Run 5. Both the horizontal and vertical scales are in centimeters.

19

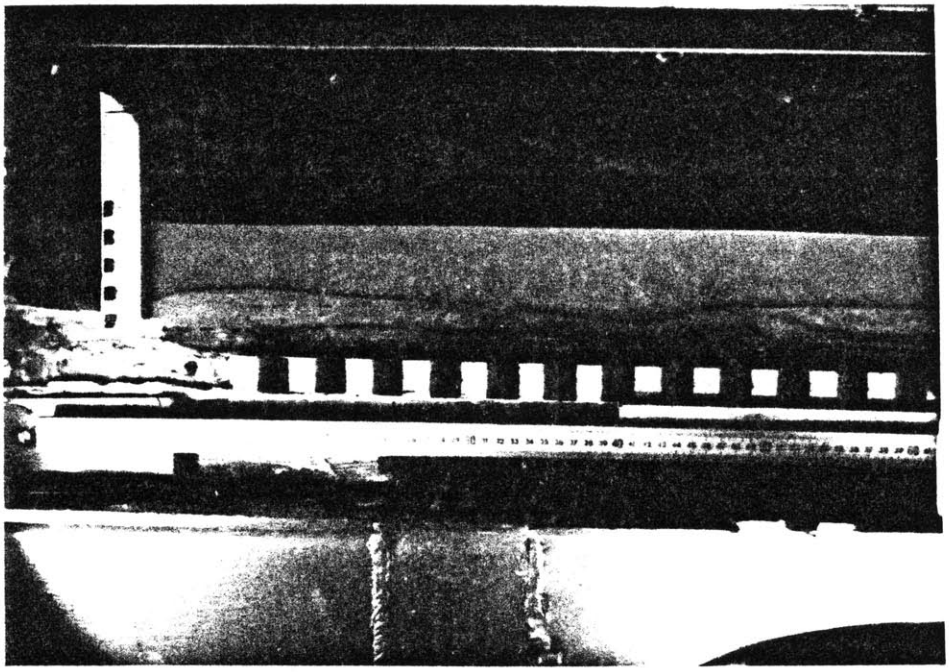

FIGURE 24: More representative ripples from Run 5. In photo 23 note the gentle slope of the slipface. Close-ups of this slipface are shown in figures 32 and 33. Horizontal and vertical scales are in centimeters. Ripple spacings are approximately 50 cm and heights are less than 2 cm.

22

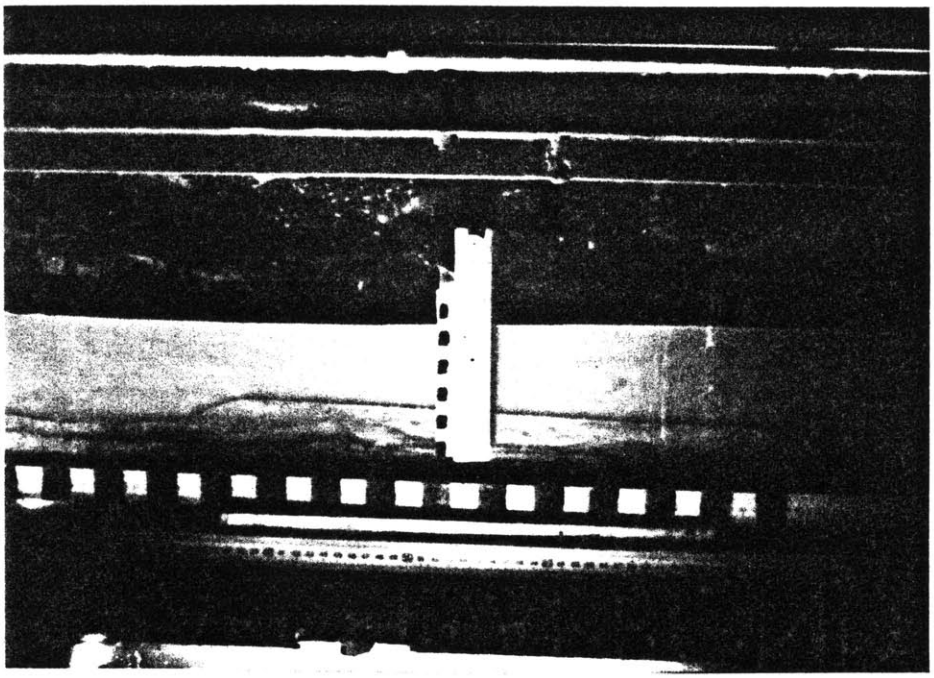

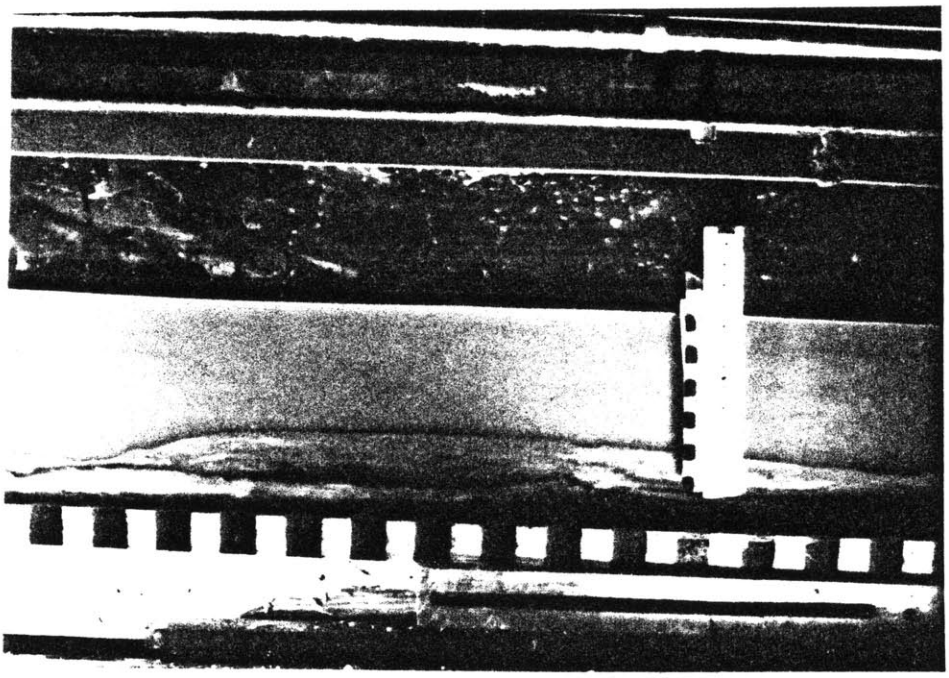

23

FIGURE 25: Typical ripples from Run 5. Note the gentle stoss and lee slopes. Both horizontal and vertical scales are in centimeters.

24

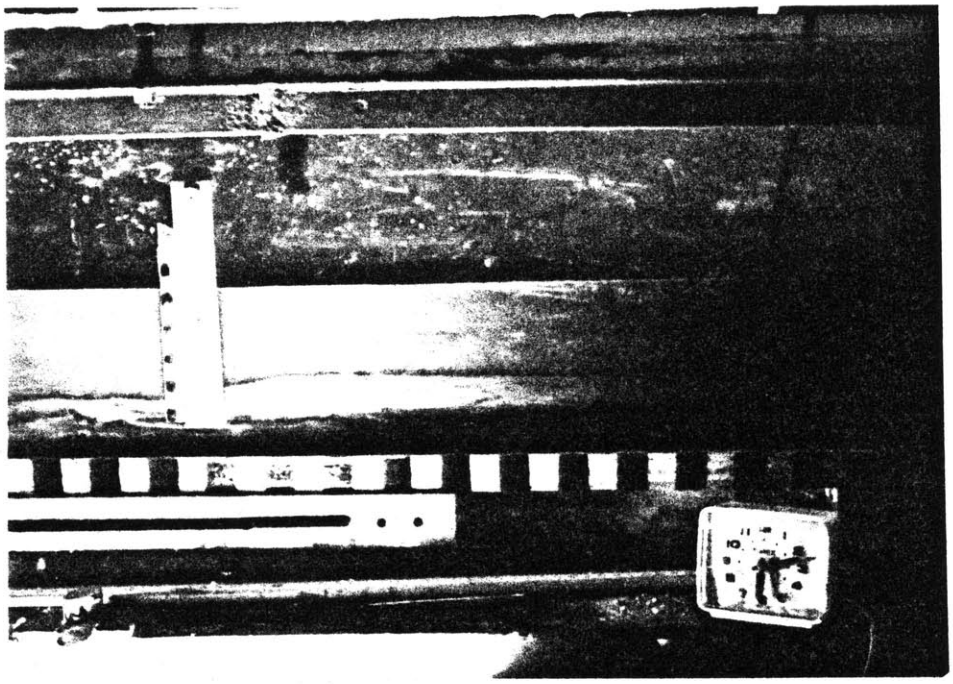

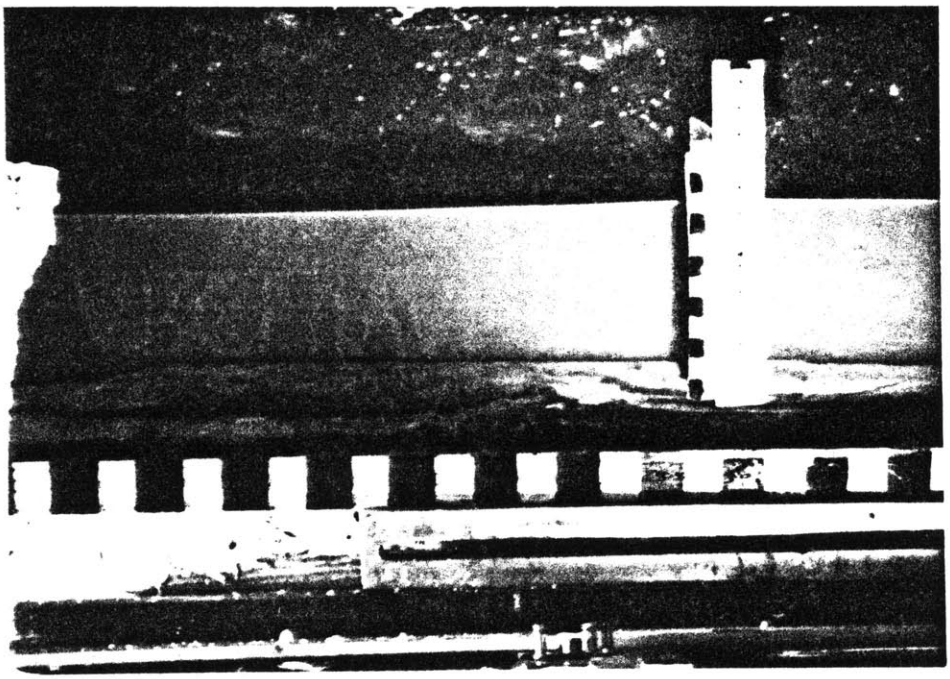

25

FIGURE 26: Additional pictures of ripples from Run 5. Photo 27 shows more accurately the spacings of the ripples. Compare these ripples with ripples from Run 1. Though the lengths are similar, the heights differ by a factor of three.

26

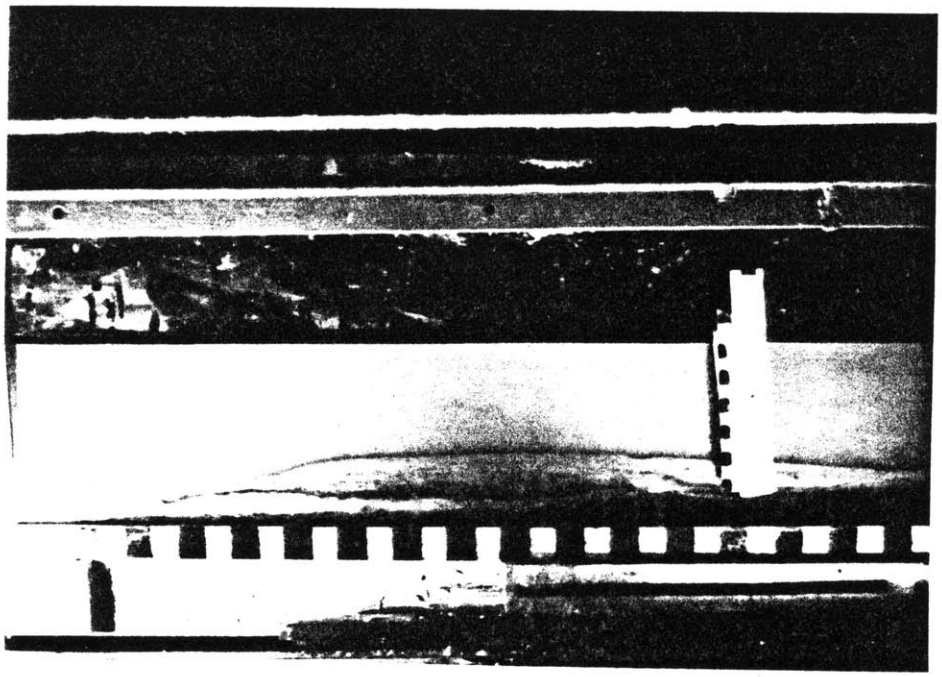

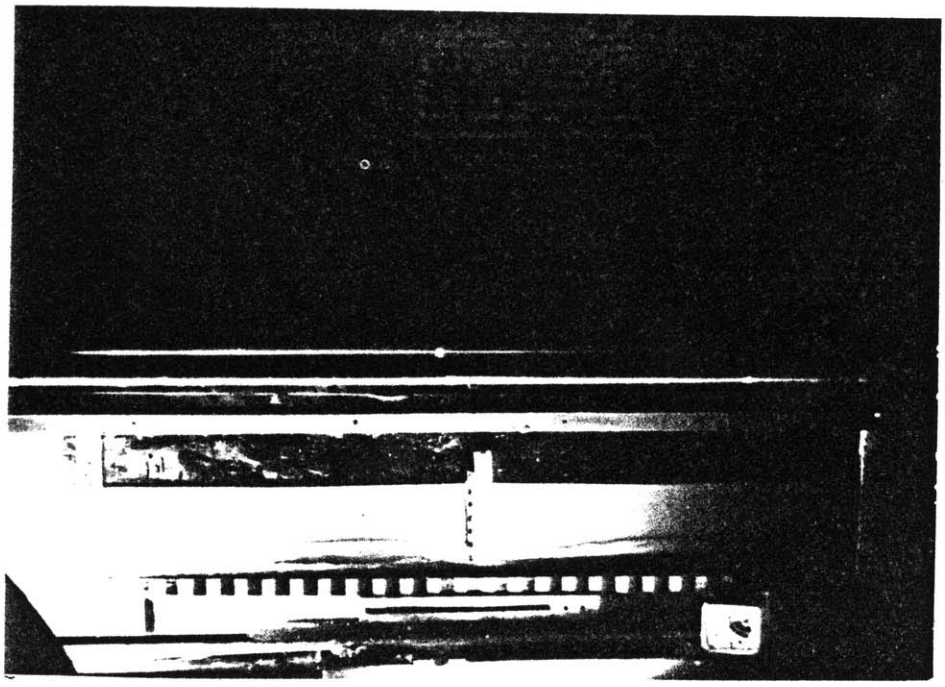

27

slipface angle was 14.8°, greatly different than in Runs 3 and 4 and only half the mean angle noted in Run 2. Migration rate was 0.03 cm/min and ripple height and spacing were 0.31 and 9.3 cm, respectively. Ratio of suspended to bed load transport was approximately 4.4, and in this run most sediment accreting on the lee slope did so through bed-load movement with subsequent avalanching of grains.

LAMINATION

Ripple morphology was similar in Runs 1 through 5, and not surprisingly the lamination produced was similar as well. The lamination was all small-scale trough cross-stratification. Figures 14 and 28 from Run 1 show some of the typical stratification. Figure 29 is an example from Run 2, and Figure 31 from Run 4. Both show stratification equivalent to that in Run 1. Figure 27, photograph 5 and Figure 28, Figure 21, Figures 32 and 33 and Figures 34, photograph 32 show the avalanching of grains down the planar lee slope from Runs 1, 4, 5 and 6, respectively. Note that avalanching was similar in all runs, and in some of the photos, particularly 7 and 8, the slumping grains moved as a unit with a mini-ripple-like morphology in profile.

FIGURE 27: Profiles of ripples from Run 1. Photo 5 shows slumping occurring on the lee face of a ripple. Note the size of the ripple in photo 6. This particular ripple was nearly 120 cm long and 7.3 cm high.

5

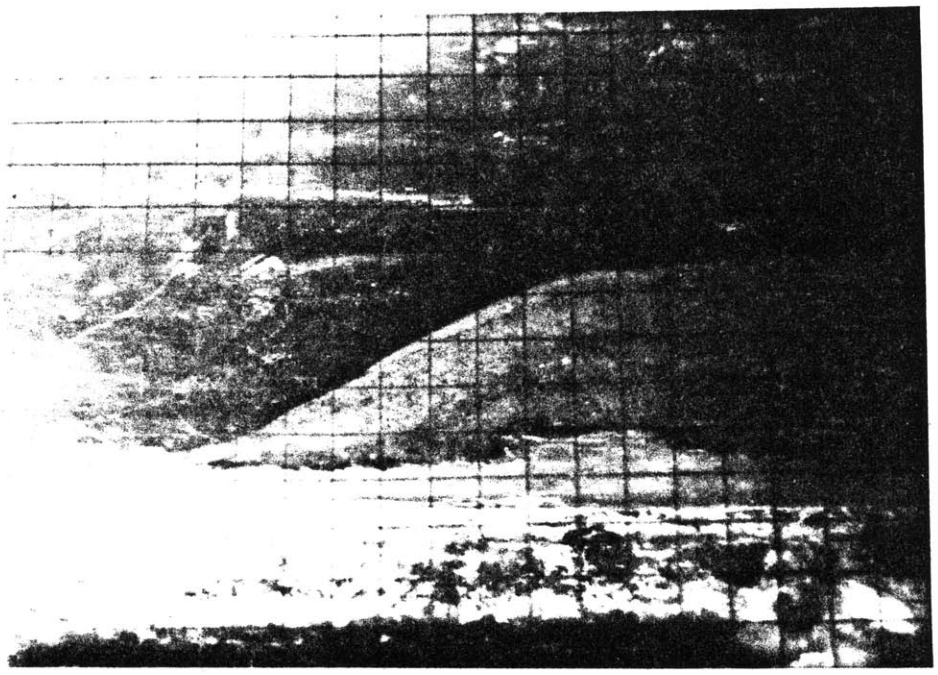

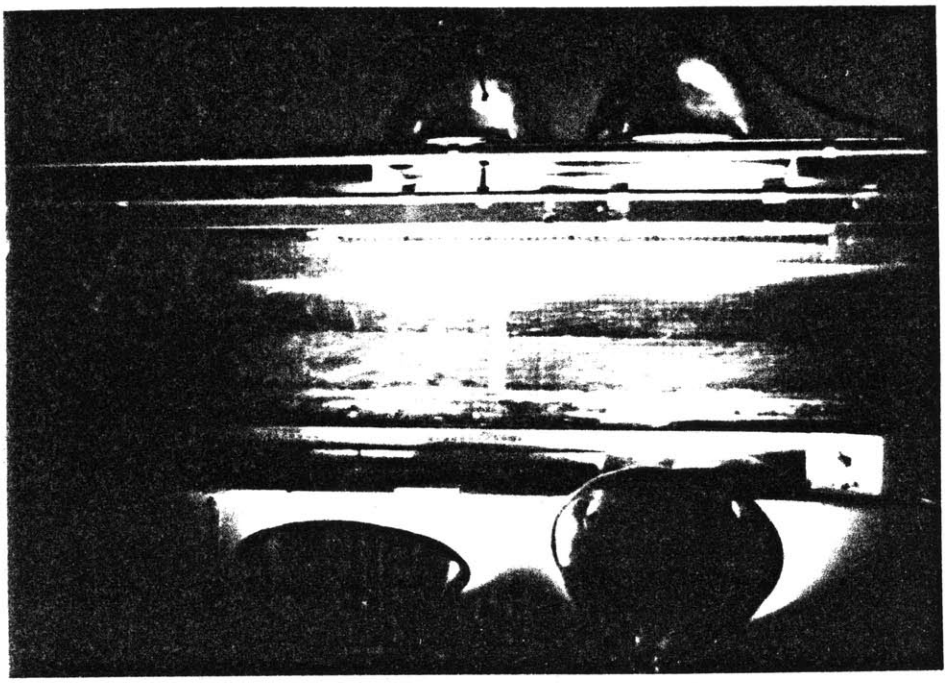

6

FIGURE 28: Both photos are of ripple lee slopes from Run 1. The grid in the photos is in 1 cm by 1 cm units. In both ripple slipfaces note the lamination and the active slumping.

7

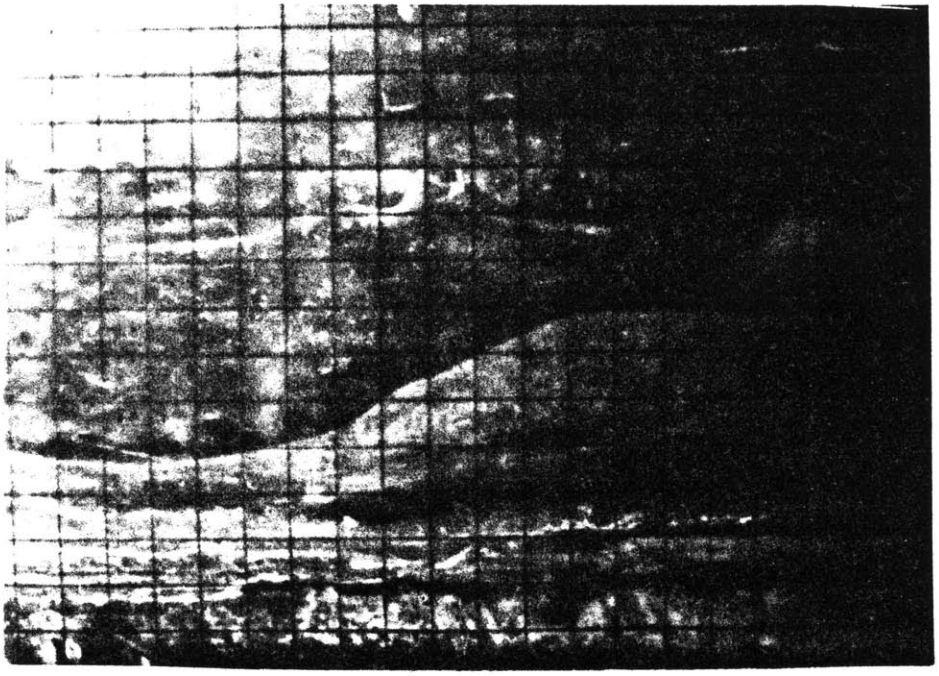

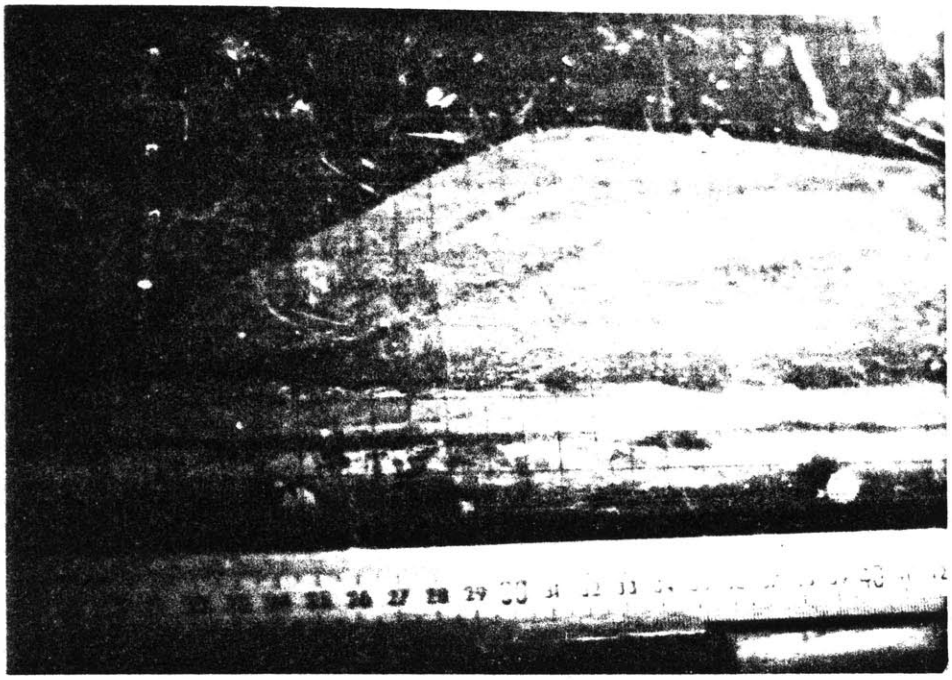

8

FIGURE 29: Two examples of ripple stratification from Run 2.

11

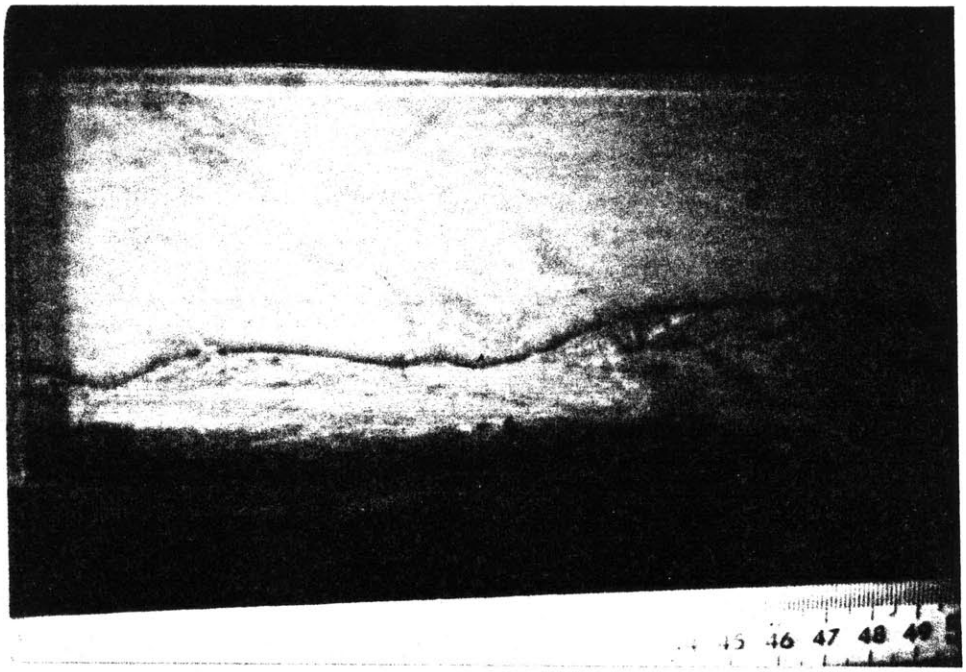

12

FIGURE 30: Some lamination can be seen in this photo of a lee face from Run 4. The scale consists of 2 cm gradations.

28

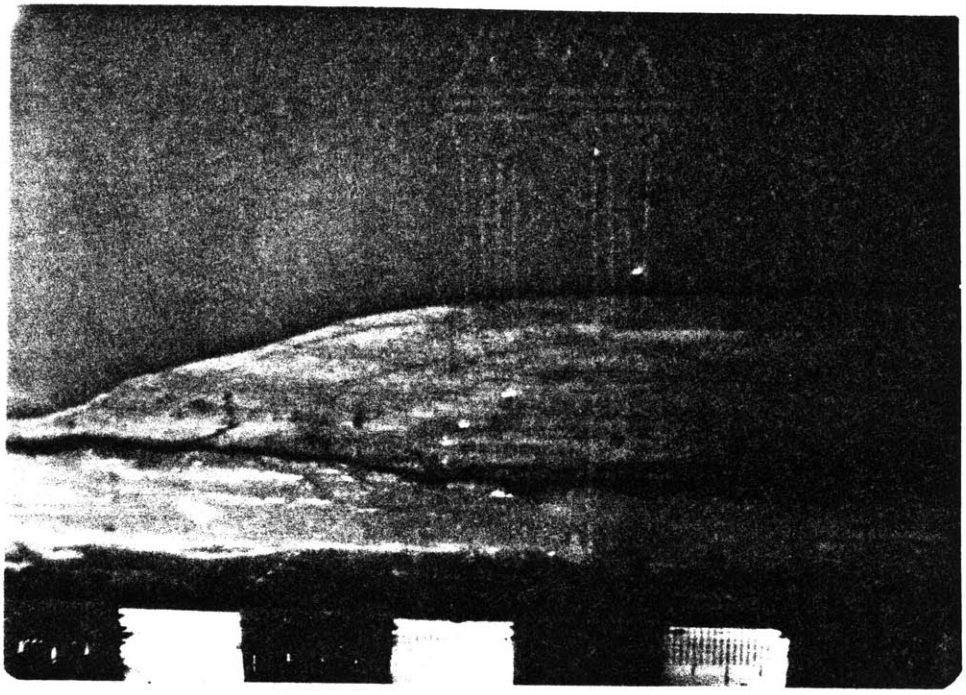

FIGURE 31: Examples of ripple morphology and stratification from Run 4. The bottom scale is in 2 cm gradations, the vertical scale in 1 cm intervals.

20

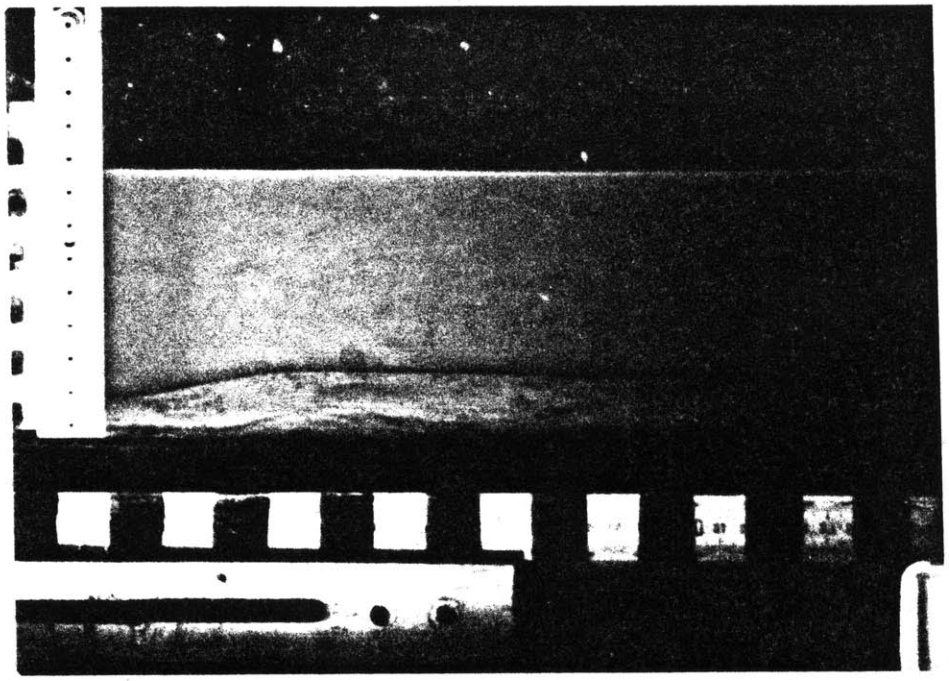

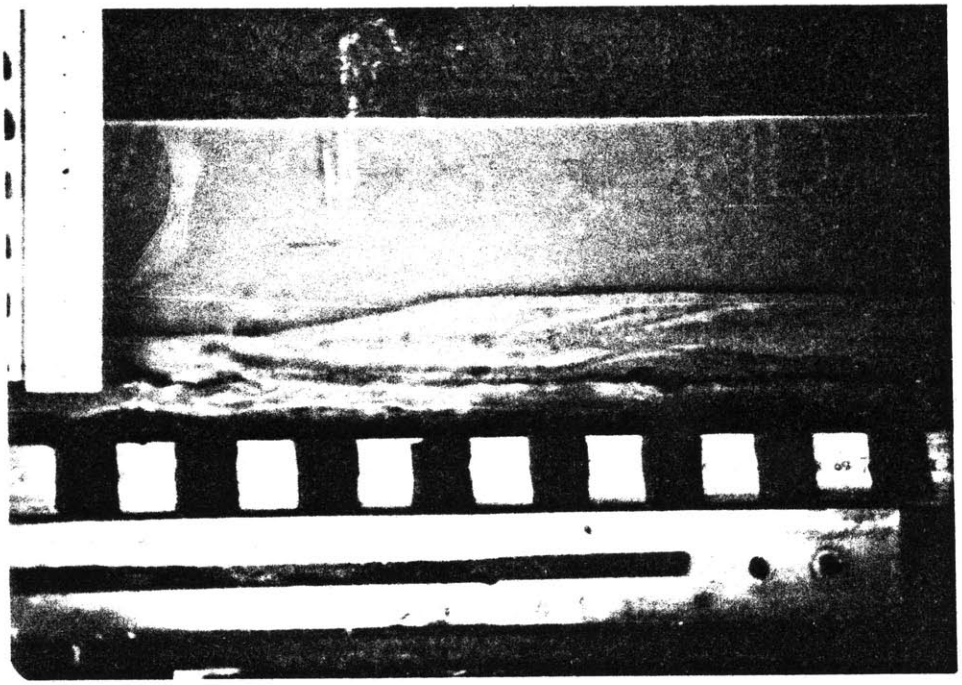

21

FIGURE 32: Close-up of a slipface from Run 5. Note that the slipface angle in this picture is approximately 15°.

17

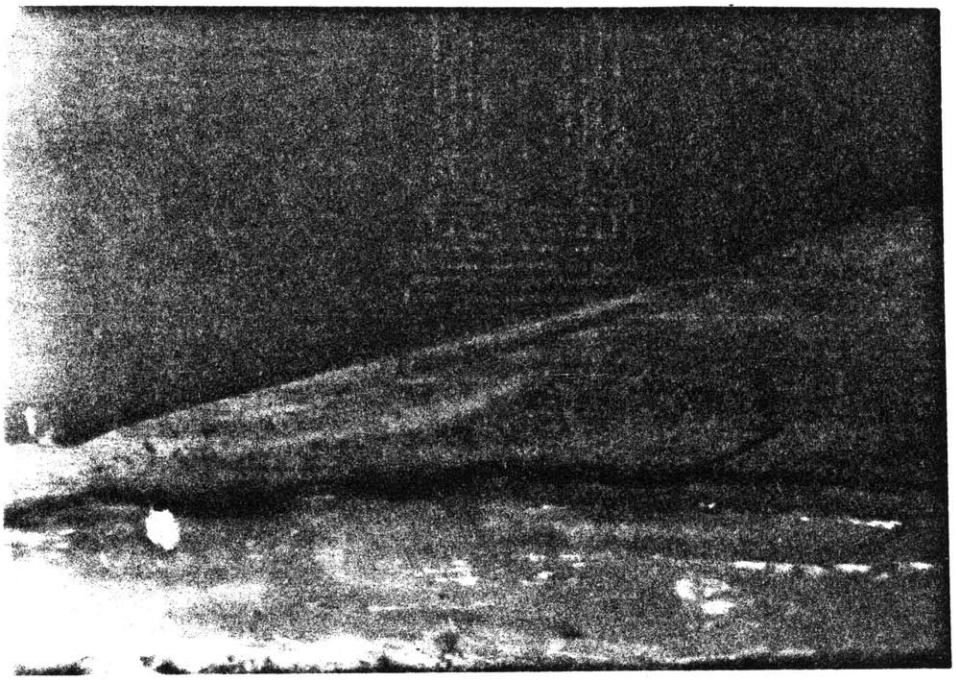

FIGURE 33: Close-up of the bottom of the slipface from the previous picture. Note the slumping in the center of the picture. Scale in 2 cm intervals.

18

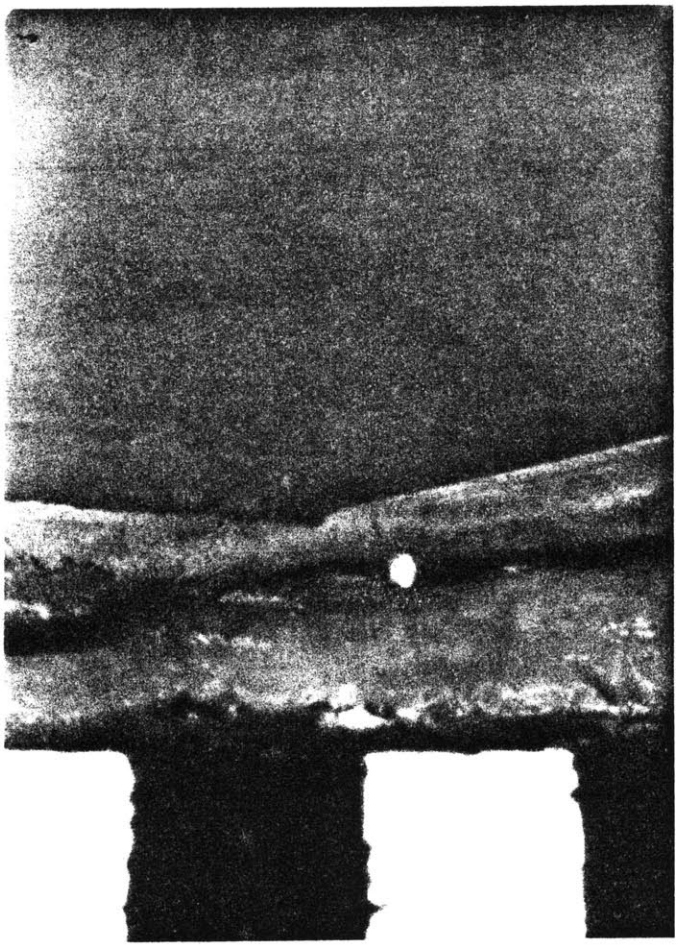

FIGURE 34: Ripple profiles from Run 6. Note the slumping in photo 32. Scale is in 2 cm gradations.

31

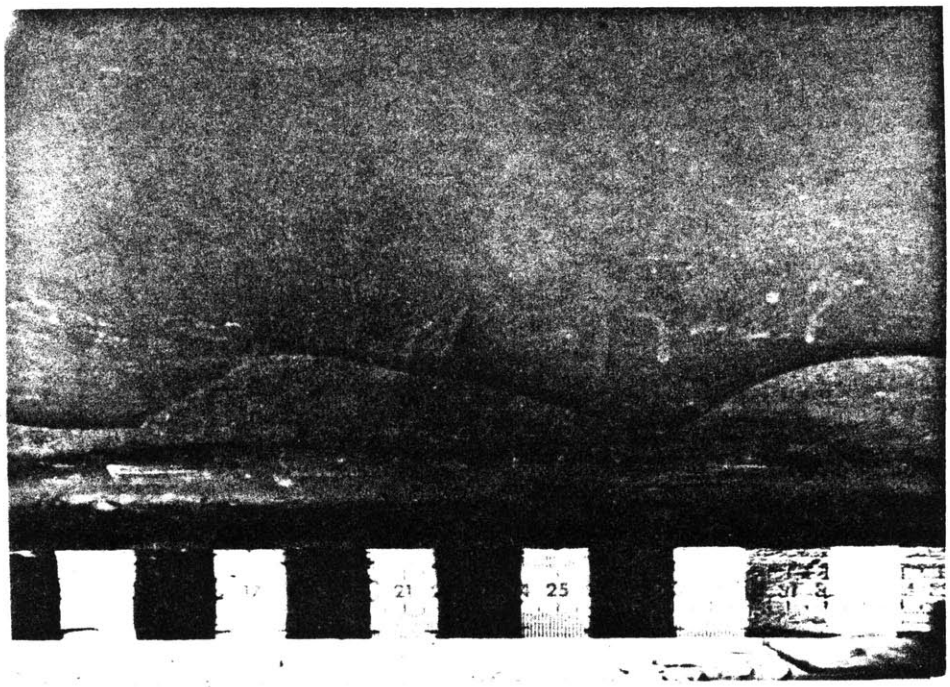

32

DISCUSSION

RIPPLE MORPHOLOGY

Frequency curves plotted in Figures 20, 21, and 22 for spacing, height, and migration rates in Runs 3, 4, and 5 suggest some general relationships. When viewing these diagrams it is helpful to remember that with increasing run number, effective grain size drecreases (Table 3). The frequency curve for spacing (Fig. 20) shows that a minimum average ripple spacing exists, despite variations in grain sizes. However in these runs it must be remembered that effective flow depth is less than 3 cm and flow velocity varies between 24 cm/s and 37 cm/s thus similar spacings for ripples due to variations in grain size may be due to the limited range in variables tested. Figures 35 and 37 are graphs of flow velocity U vs spacing L and grain size D vs spacing L, respectively. Data from Runs 2 - 5 and from runs in previous studies (Jopling and Forbes, 1979; Mantz, 1980) are presented in Figures 35 and 37. In Figure 35, U vs L, a minimum ripple spacing of approximately 8 cm exists over a range of flow velocity from 10 to 56 cm/s. In Figure 37, minimum ripple spacing occurs at spacings of approximately 9 cm. Since only three other sediment sizes finer than 48 m are plotted, one can only tentatively suggest that a minimum ripple spacing exists with decreasing grain size.

Ripple height frequency curves for Runs 3 - 5 are presented in Figure 21. One can clearly see a strong trend of decreasing ripple height with decreasing sediment size. Since ripple spacing remains essentially constant, it follows that ripple index increases with decreasing grain size (Appendix 2). Indeed ripple indexes increase from values of 10 and 12 for the early runs to a value of 31.5 for Run 5.

Variation of ripple heights with flow velocity and mean grain diameter using data from Jopling and Forbes (1979) and Mantz (1980) are presented in Figures 36 and 38. Too much scatter exists in the graph of velocity versus height to draw any conclusions from it except that a broad range of heights are stable within a wide range in flow velocities. In Figure 38, one is again confronted by the lack of data points; however, even with the points presented, a strong trend of decreasing ripple height with decreasing grain diameter is readily observable. Since ripple heights in sands are generally less than 4 cm, it is apparent that the curve must exhibit exponential growth since a stable ripple height of 1 to 4 cm must be quickly reached. Figure 38 suggests that at extremely small grain sizes, a minimum ripple height of approximately 0.2 cm is reached.

A plot of mean ripple migration rate versus grain size is presented in Figure 39. Generally speaking, migration rate increases linearly with grain size, and a similar trend is seen in Figure 40 which is a plot of migration rate versus mean flow velocity

FIGURE 35: Graph of flow velocity vs ripple spacing for data obtained from this study and from the results of Jopling and Forbes (1979), and Mantz (1978; 1980).

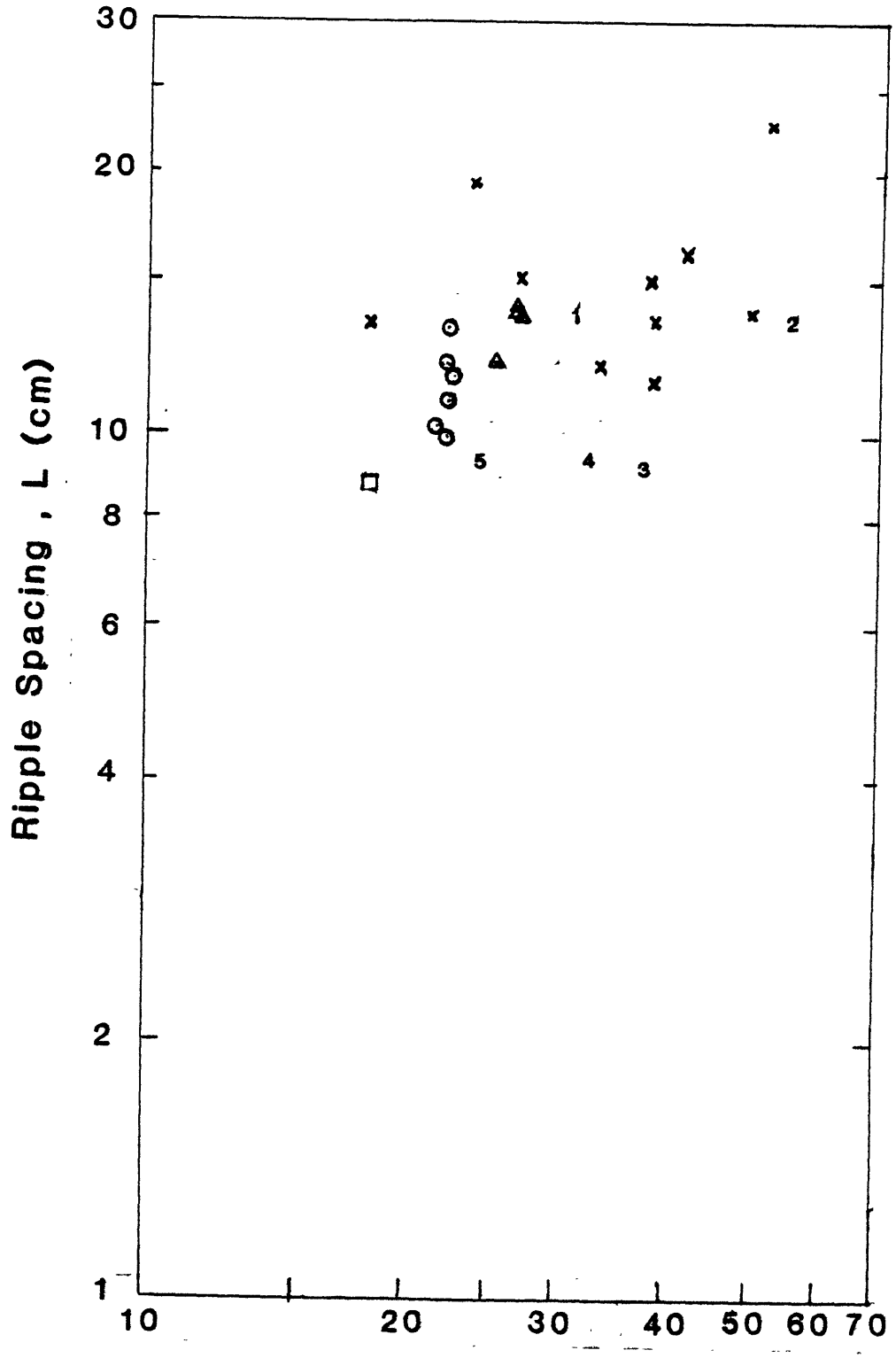

△	MANTZ (1980), 42 µm	1, 2	GRAZER	29 µm
○	MANTZ (1980), 18 µm	3	"	10 µm
□	MANTZ (1978), 15 µm	4	"	7 µm
✖	JOPLING & FORBES (1979), 45 µm	5	"	4 µm

FIGURE 36: Graph of flow velocity vs ripple height for data from this study as well as from Jopling and Forbes (1979) and Mantz (1978; 1980).

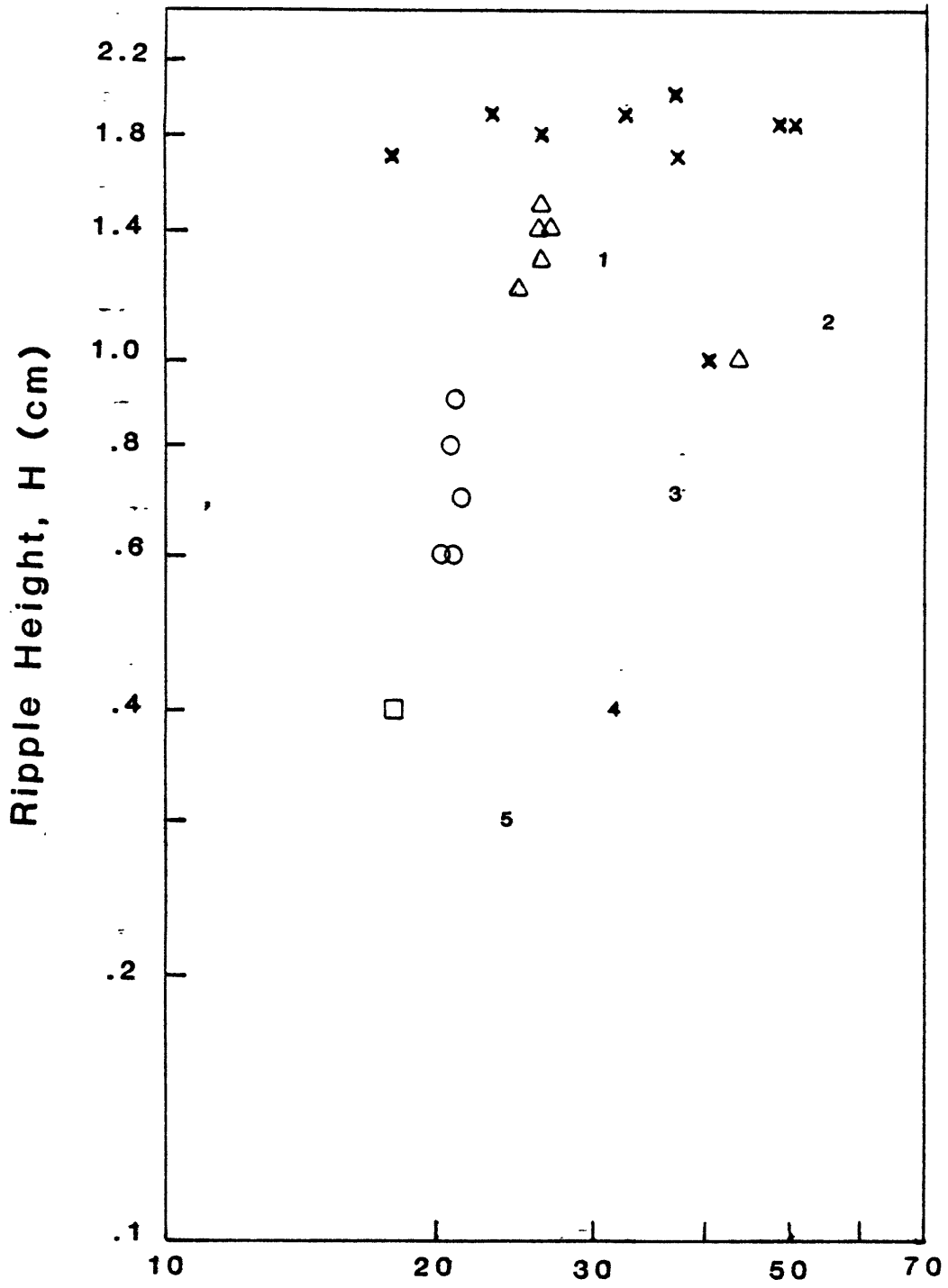

△	MANTZ (1980), 42 μm	1, 2	GRAZER	29 μm
○	MANTZ (1980), 18 μm	3	"	10 μm
□	MANTZ (1978), 45 μm	4	"	7 μm
✖	JOPLING & FORBES (1979), 45 μm	5	"	4 μm

FIGURE 37: Grain diameter vs ripple spacing for data from this study as well as from Jopling and Forbes (1979), and Mantz (1978; 1980). The points in the Jopling and Forbes, and Mantz data represent an average value for a set of runs while the bars indicate the range above and below this average value.

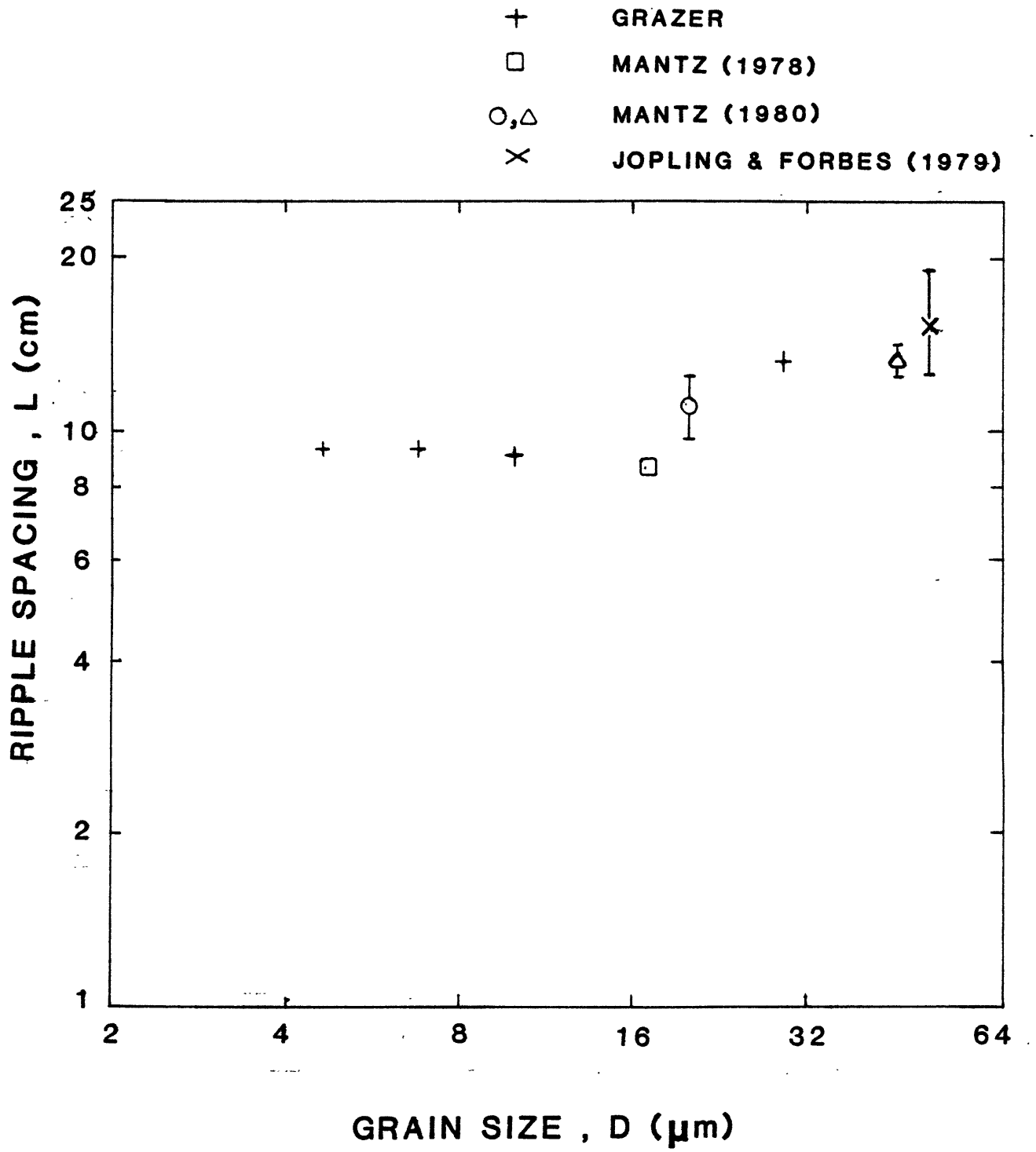
GRAZER
MANTZ (1978)
MANTZ (1980)
JOPLING & FORBES (1979)
RIPPLE SPACING , L (cm)
25
20
10
8
6
4
2
1
2
4
8
16
32
64
GRAIN SIZE , D (μm)

FIGURE 38: Ripple height vs grain diameter for data from this study, from Jopling and Forbes (1979), and from Mantz (1978; 1980). The points in the Jopling and Forbes, and Mantz data represent an average value for a set of runs while the bars indicate the range above and below this average value.

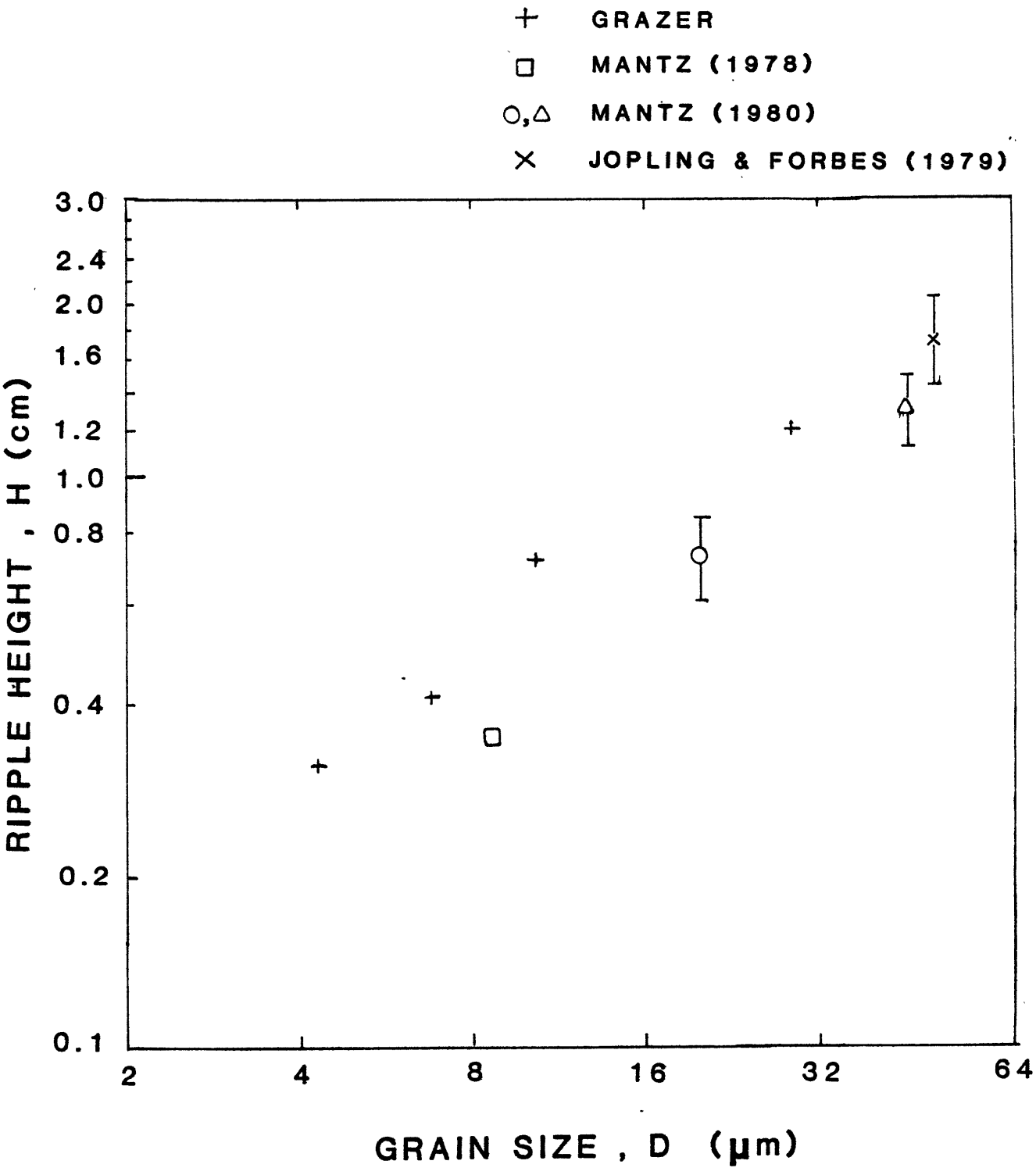
+ GRAZER
□ MANTZ (1978)
○,△ MANTZ (1980)
× JOPLING & FORBES (1979)
RIPPLE HEIGHT , H (cm)
3.0
2.4
2.0
1.6
1.2
1.0
0.8
0.4
0.2
0.1
2
4
8
16
32
64
GRAIN SIZE , D (μm)

FIGURE 39: Grain size vs migration rate for data from the present study.

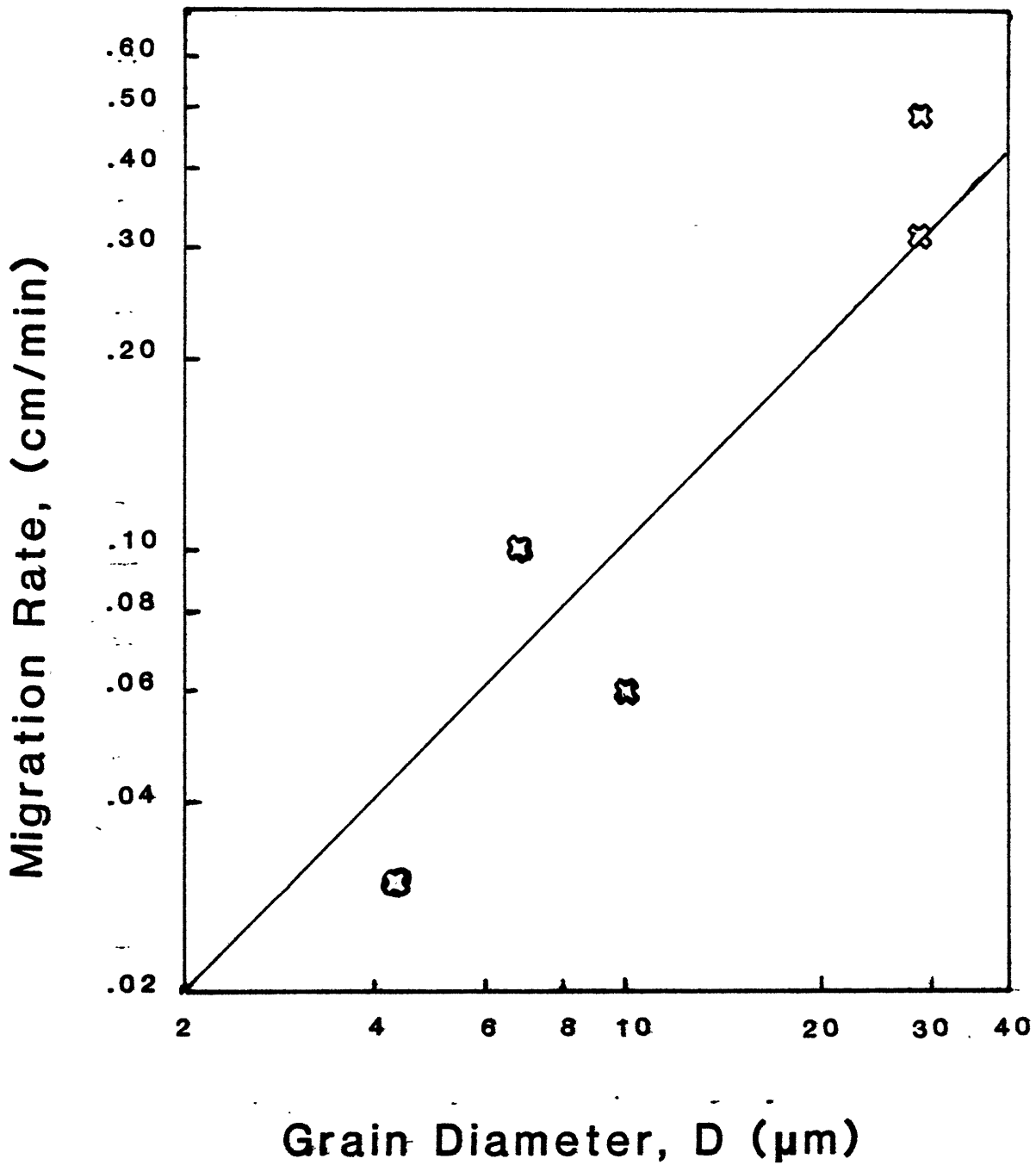
Migration Rate, (cm/min)
.60
.50
.40
.30
.20
.10
.08
.06
.04
.02
2
4
6
8
10
20
30
40
Grain Diameter, D (μm)

FIGURE 40: Flow velocity vs migration rate for data from the present study, from Jopling and Forbes (1979), from Mantz (1978; 1980), and from Banerjee (1977).

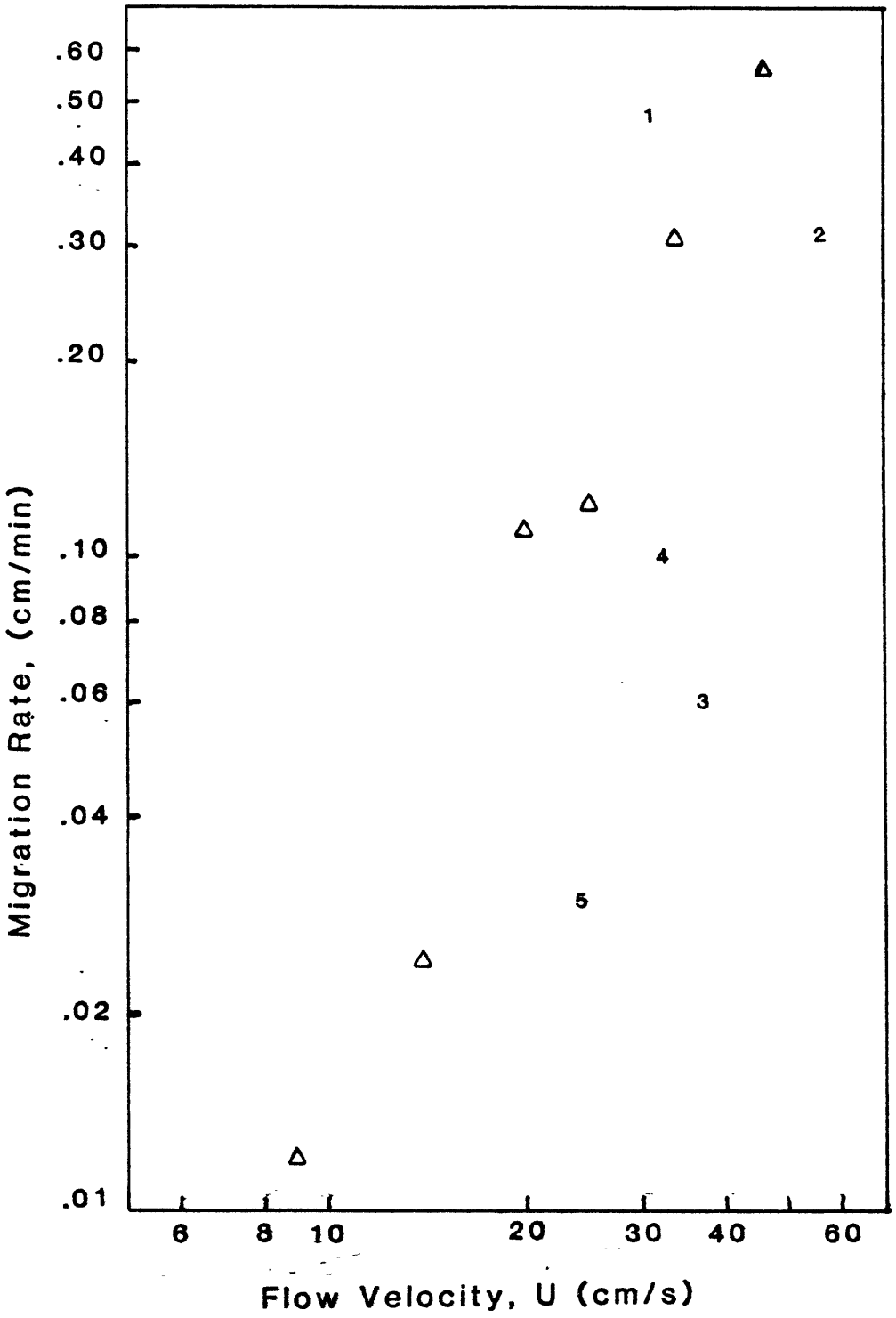

△ BANERJEE (1977), 25 μm

1, 2 GRAZER 29 μm

3 " 10 μm

4 " 7 μm

5 " 4 μm

although some additional points are needed to better define the relationship.

An interesting feature which should be noted again is the decrease in slipface angle with decreasing grain size. In Runs 1, 2 and 6, lee sides slope at approximately the static angle of repose, 30°. In Runs 3 and 4, the angle is only 22°, and in Run 5 the angle decreases further to 15°.

Thus it seems that values of ripple migration rates, ripple heights, and slipface angles decrease with decreasing mean sediment size while ripple spacing approximately attains a minimum value of 8 to 9 cm.

SEDIMENT TRANSPORT

Scaled sediment-transport data for Runs 1 - 6 are presented in Figure 40 and Table 4. Figure 40 displays the trend of increasing suspended and total sediment transport with increasing bed shear stress. These results compare favorably with results presented by Kalinske and Hsia (1945). Kalinske and Hsia contend that bed-load transport is insignificant for a wide variety of flow states, including those in which ripples are found. Data given in Table 4 suggests that bed-load transport is minor relative to suspended-load transport in Runs 1 and 2 but bed-load becomes increasingly important in Runs 3 through 6 as the ratio of suspended to bed-load transport rate decreases from approximately 7 in Runs 3 and 4 to 4 in Run 5 and 2.5 in Run 6.

FIGURE 41: Graph of suspended and total sediment transport vs bed shear stress for Runs 1-6.

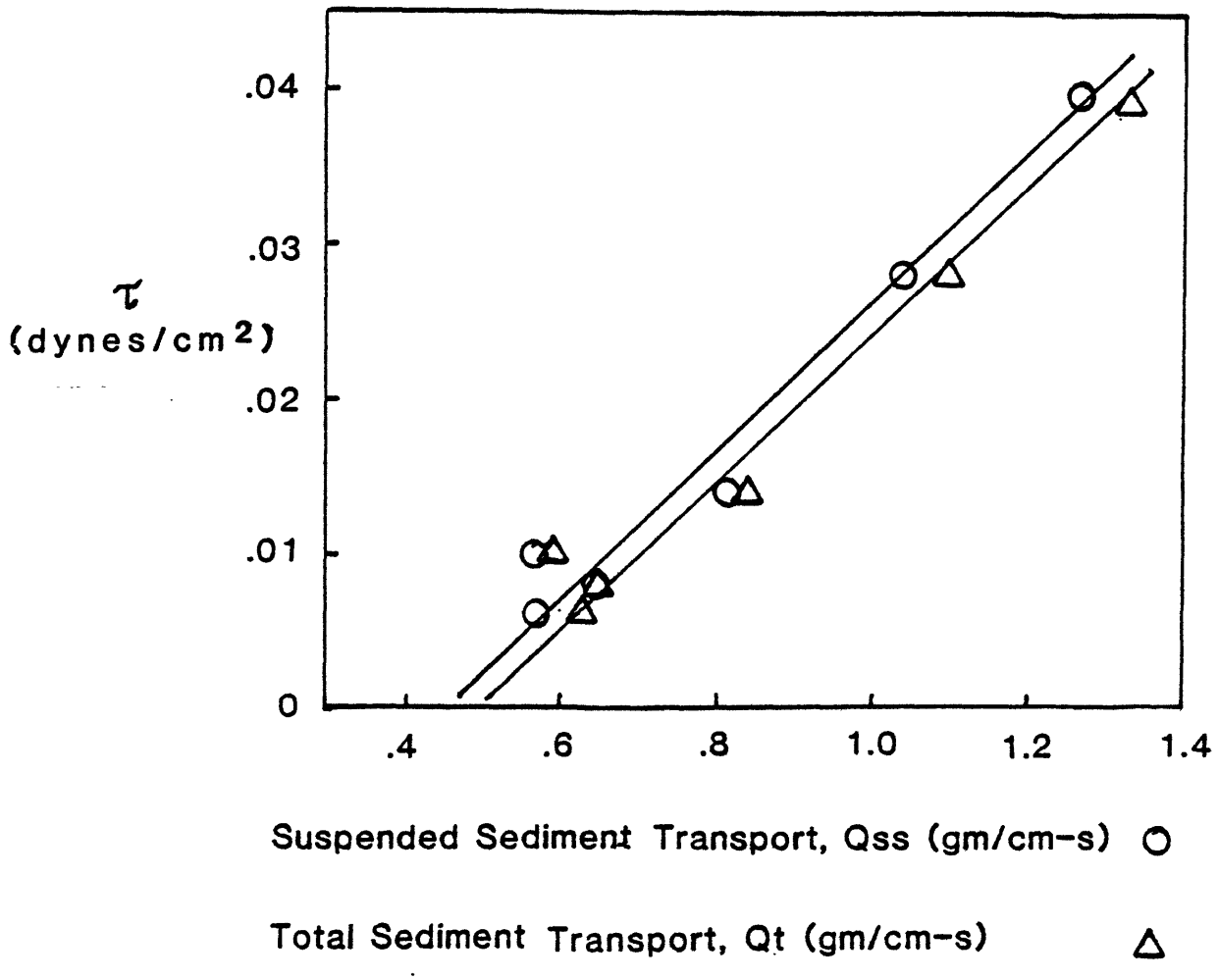
.04
.03
τ
(dynes/cm 2)
.02
.01
0
.4
.6
.8
1.0
1.2
1.4
Suspended Sediment Transport, Qss (gm/cm-s)
Total Sediment Transport, Qt (gm/cm-s)

LAMINATION

Stanley (1974) examined Quaternary lake silt lamination in Nebraska. He found one unusual feature, that being micro-ripples superimposed on the stoss sides of larger ripples. These larger ripples ranged in spacing from 15 to 60 cm and in height from 2 to 6 cm. Stanley named this particular type of lamination micro-ripple-drift cross-lamination but was unable to account for the origin of such features.

In the present study, cross-laminae existed throughout the runs and were lenticular or tabular in shape. The cross-laminae delineating the internal structure of the ripples were well defined, especially in Runs 1 and 2 (Figures 14 - 18). The thickness of the individual laminae throughout the runs were on the order of 0.1 mm.

Based on observations on ripple movement and origin of laminae, it is proposed that Stanley's micro-ripples were in effect groups of grains moving in ripple-like fashion down the lee slopes of ripples and up the stoss slopes of the next ripples downstream. Figures 28 and 33 present some typical micro-ripple-like features active in slumping of grains down the lee slopes of the ripples.

Stanley reveals that the micro-ripple-drift laminae were formed on ripples of unusually large size. He noted that the silts were deposited in a glacial area by density currents flowing into a small shallow lake. These are ideal conditions for natural Reynolds-Froude modeling

producing scaled-up models of ripples. The water was colder than normal and suspended sediment was high, both factors contributing to higher-than-normal fluid viscosity. Stanley was seeing scaled-up small features responsible for slumping and scaled-up ripples due to the high viscosity of the fluid which was present in the natural environment.

SUMMARY

Having proven the effectiveness of Reynolds-Froude scaled-up modeling, runs were made at different scale ratios to study differences in ripple morphology or dynamics with variations in effective mean grain size. The data suggests that a minimum mean ripple spacing exists, that ripple heights and slipface angles decrease with decreasing grain size, and ripple index increases as sediment becomes finer.

Both suspended and bed-load transport rates are important in ripple migration, and suspended loads are 4 to 7 times greater than bed-load rates. Ripple lamination in the runs consisted of small-scale trough stratification, with individual laminae being tabular or lenticular in shape.

The origin of Stanley's (1974) micro-ripple-drift cross-stratification can be explained neatly assuming that increased viscosities resulting from high suspended sediment loads and cold glacial water effectively scaled up ripples in silt and these micro-ripples were in fact, groups of grains which avalanched down the lee-side together, though appearing to be something else due to the scale ratio in the flow system.

It is possible that many of the anomalous ripple size values reported in the literature may be due to anomalously high viscosity values for the fluid shaping the

ripples. Since viscosity allows one to manipulate other sedimentologically important variables easily, it is hoped that future flume studies will use viscosity more effectively than it has been used in the past.

Appendix 1

Theoretical Calculation of Discharge

$$q = k_1 P^{\frac{1}{2}} \qquad k_1 = [\pi^2/8\ \rho_w (1/D_2^4 - 1/D_1^4)]^{\frac{1}{2}}$$

P=pressure difference

$\rho_w = 1.00$ gm/cm^3

D_1=diameter of return pipe=5.2 cm

D_2=diameter of orifice meter=3.5 cm

$$k_1 = 15.26$$

$$q = 15.26(P)^{\frac{1}{2}} \text{ cm}^3/\text{s}$$

$$q = k_1[(\rho_m - \rho_w) g\ Hg]^{\frac{1}{2}}$$

ρ_m=density of mercury=13.6 gm/cm^3

$g = 980$ cm/s^2

$q = 1696(Hg)^{\frac{1}{2}}$ Hg=difference in mercury levels in manometer

For	$\rho = 1.204$ gm/cm^3	$q = 1682(Hg)^{\frac{1}{2}}$ cm^3/s
	$\rho = 1.131$ gm/cm^3	$q = 1687(Hg)^{\frac{1}{2}}$ cm^3/s
	$\rho = 1.176$ gm/cm^3	$q = 1683(Hg)^{\frac{1}{2}}$ cm^3/s
	$\rho = 1.220$ gm/cm^3	$q = 1681(Hg)^{\frac{1}{2}}$ cm^3/s

Note: Negligible difference in discharge among fluids used in these experiments

APPENDIX 2

Summary of Flume Data

TABLE 5

Unscaled Experimental Data: Run 1

Ripple #	Velocity cm/s	Rate cm/min	Height cm	Length cm	Depth cm	Lee Angle	Ripple Index
1	61.9	1.035	4.6	58.6	11.2	26.0	12.7
2		0.934	5.7	55.9		29.4	9.8
3		0.905	4.3	58.0		29.2	13.5
4		0.538	7.3	117.3		29.4	16.1
5		0.644	7.3	56.3		31.0	7.7
6		1.162	5.5	32.0		26.0	5.8
7		1.320	4.7	32.0		29.5	6.8
8		1.246	4.2	31.8		29.7	7.6
9		0.877	4.5	46.9		29.0	10.4
10		0.851	5.5	89.1		29.0	16.2
11		0.996	4.3	32.3		28.0	7.5
12		1.139	4.8	46.3		30.5	9.6
13		0.940	4.8	46.1		30.3	9.6
14		0.936	3.8	43.6		30.5	11.5
$\bar{X}$		0.966	5.1	53.3		29.1	10.3
SD		0.213	1.1	24.0		1.5	3.3

TABLE 6

Unscaled Experimental Data: Run 2

Ripple #	Velocity cm/s	Rate cm/min	Height cm	Length cm	Depth cm	Lee Angle	Ripple Index
1	47.5	0.40	0.85	9.1	4.7	25.5	10.7
2		0.43	0.56	8.4		29.6	15.0
3		0.23	0.47	8.6		27.4	18.3
4		0.19	0.54	8.1		31.2	15.0
5		0.10	0.84	8.5		33.1	10.1
6		0.19	1.60	13.1		28.5	8.2
7		0.24	1.25	9.4		29.0	7.5
8		0.25	0.58	9.8		28.4	16.9
9		0.23	0.62	8.2		26.3	13.2
10		0.31	0.73	8.5		28.4	11.7
$\bar{X}$		0.26	0.80	9.2		28.7	12.7
SD		0.10	0.36	1.5		2.2	3.6

TABLE 7

Unscaled Experimental Data: Run 3

Ripple #	Velocity cm/s	Rate cm/min	Height cm	Length cm	Depth cm	Lee Angle	Ripple Index
1	52.9	0.16	1.60	20.3	4.8	22.5	12.7
2		0.11	1.46	18.9		23.2	12.9
3		0.07	1.38	15.0		19.8	10.9
4		0.04	1.22	17.0		19.5	13.9
5		0.05	1.43	19.3		21.0	13.5
6		0.08	1.51	18.7		23.2	12.4
7		0.10	1.33	17.5		26.1	13.2
$\bar{X}$		0.09	1.42	18.1		22.2	12.8
SD		0.04	0.12	1.8		2.3	1.0

TABLE 8

Unscaled Experimental Data: Run 4

Ripple #	Velocity cm/s	Rate cm/min	Height cm	Length cm	Depth cm	Lee Angle	Ripple Index
1	56.1	0.16	1.63	27.2	7.3	23.3	16.7
2		0.20	0.88	22.0		18.5	25.0
3		0.16	1.10	30.0		22.1	27.3
4		0.22	1.19	27.1		19.6	22.8
5		0.20	1.05	27.8		17.4	26.5
6		0.14	1.55	32.5		27.0	21.0
7		0.17	1.20	30.1		24.3	22.8
8		0.19	1.26	26.2		23.1	20.8
$\bar{X}$		0.18	1.23	27.9		21.9	22.9
SD		0.03	0.23	3.1		3.2	3.4

TABLE 9

Unscaled Experimental Data: Run 5

Ripple #	Velocity cm/s	Rate cm/min	Height cm	Length cm	Depth cm	Lee Angle	Ripple Index
1	52.7	0.10	1.6	51.2	7.6	14.3	32.0
2		0.09	2.1	54.7		13.5	26.0
3		0.02	1.0	45.5		16.4	45.5
4		0.05	1.4	33.4		14.3	23.9
5		0.04	1.4	36.3		13.2	25.9
6		0.04	1.3	46.6		17.1	35.8
$\bar{X}$		0.06	1.5	44.6		14.8	31.5
SD		0.03	0.4	8.3		1.6	8.2

TABLE 10

Unscaled Experimental Data: Run 6

Ripple #	Velocity cm/s	Rate cm/min	Height cm	Length cm	Depth cm	Lee Angle	Ripple Index
1	59.7	3.02	1.2	9.1	12.7	35.0	7.6
2		1.43	1.2	10.3		31.2	8.6
3		0.95	1.4	18.4		33.1	13.1
4		1.20	1.7	19.1		32.2	11.2
5		2.66	0.8	11.5		33.3	14.4
6		2.08	1.2	13.2		31.1	11.0
7		2.21	1.9	12.1		26.5	6.4
8		1.84	1.3	12.2		33.4	9.4
9		1.69	0.8	12.4		36.0	15.1
10		0.83	2.7	18.6		34.3	6.9
11		1.11	2.2	15.7		36.5	7.1
12		1.47	1.8	10.3		33.1	5.7
13		1.88	1.3	15.1		30.2	11.6
14		2.71	1.1	15.0		29.7	13.6
15		2.43	1.2	10.0		31.4	8.3
16		1.76	2.5	11.2		29.6	4.5
17		1.11	1.7	11.1		30.1	6.5
18		1.07	1.6	10.4		33.2	6.5
19		2.64	2.1	15.1		34.5	7.2
20		2.32	2.2	15.4		32.1	7.0
21		1.48	1.4	13.7		30.7	9.8
22		2.85	0.9	9.5		33.6	10.6
23		2.97	1.9	9.5		36.0	5.0
24		1.56	2.2	10.0		32.2	4.5
25		1.60	1.4	16.2		30.8	11.6
26		2.02	1.8	12.1		34.9	6.7
27		2.32	2.0	14.7		36.1	7.3
28		2.41	1.5	11.5		32.1	7.7
29		2.91	1.0	7.2		29.3	7.2
30		3.08	1.5	7.5		30.2	5.0
31		3.10	0.7	6.6		29.1	9.4
$\bar{X}$		2.02	1.6	12.4		32.3	8.6
SD		0.70	0.5	3.3		2.4	2.9

REFERENCES

Allen, J.R.L., 1968, Current ripples: their relations to patterns of water and sediment motion, North Holland Publ. Co., Amsterdam, 433 pp.

Allen, J.R.L., 1970, Physical processes of sedimentation, George Allen and Unwin Ltd, London, 248 pp.

Bagnold, R.A., 1966, An approach to the sediment transport problem from general physics, U.S.G.S. Prof. Paper 422-I, p. 1-37.

Banerjee, I., 1977, Experimental study on the effect of deceleration on the vertical sequence of sedimentary structures in silty sediments, J. Sed. Pet., 47, 771-783.

Boguchwal, L.A., 1977, Dynamic scale modeling of bed configurations, Thesis (Ph.D.) MIT, 1977.

Boswell, P.G.H., 1961, Muddy sediments: some geotechnical studies for geologists, engineers and soil scientists, W Heffer & Sons Ltd. Cambridge, 140 pp.

Buckingham, E., 1914, On physcially similar systens; illustrations of the use of dimensional equations, Physical Review, lV, no. 4, p. 345-376.

Daily & Harleman, D.R.F., 1966, Fluid dynamics, Addison-Wesley Publishing Company Inc., Massachusetts, 454 pp.

Dillo, H., 1960, Sandwanderung in Tideflussen, mitteilungen des Francius-Institute fur grund und Wasserbau, Technische Hochschule, Hanuover, p. 135-253.

Handbook of Chemistry and Physics, 1975, R. Weast, ed., 56th edition, Chemical Rubber Co. Press.

Harms, J.C., 1969, Hydraulic significance of some sand ripples, Bull. Geological Soc. Am. 80, 363-396.

Jopling, A.V., and Forbes, D.L., 1979, Flume study of silt transportation and deposition, Geografiska Annaler, 61 A, 1-2, 67-83.

Kalinske, A.A., and Hsia, C.H., 1945, Study of transportation of fine sediments by flowing water, University of Iowa Studies in Engineering, 3-34.

Mantz, P.A., 1977, Packing and angle of repose of naturally sedimented fine silica solids immersed in naturally aqueous electrolytes, Sedimentology, 24, 819-832.

Mantz, P.A., 1978, Bedforms produced by fine, cohesionless, granular and flakey sediments under subcritical water flows, Sedimentology, 25, 83-103.

Mantz, P.A., 1980, Laboratory flume experiments on the transport of cohesionless silica silts by water streams, Proc. Instn. Civ. Engrs, part 2, 69, 977-994.

Rees, A.I., 1966, Some flume experiments with a fine silt, Sedimentology, 25, 83-103.

Royse, C.F., 1970, An introduction to sediment analysis, Arizona State University, 180 pp.

Southard, J.B., 1971, Representation of bed configurations in depth-velocity-size diagrams. J. Sed. Pet., 41, 903-915.

Southard, J.B., and Harms, J.C., 1972, Sequence of bedform and stratification in silts, based on flume experiments. Am. Assoc. Pet. Geol. Bull., 56, 654-655.

Southard, J.B., Boguchwal, L.A., and Romea, R.D., 1980, Test of scale modeling of sediment transport in steady unidirectional flow, Earth Surface Processes, 5, 17-23.

Stanley, K.O., 1974, Morphology and hydraulic significance of climbing ripples with superimposed micro-ripple-drift cross-lamination in lower Quaternary lake silts, Nebraska, J. Sed. Pet., 44, 472-483.

Williams, G.P., 1970, Flume width and water depth effects in sediment transport experiments, U.S. Geol. Survey Prof. Paper 562-H, 37 pp.

Yalin, M.S., 1977, Mechanics of sediment transport, Pergamon Press, Oxford, 295 pp.

Young, R.A., 1975, Flow and sediment properties influencing erosion of fine-grained marine sediments: sea floor and laboratory experiments, Thesis (Ph.D) MIT-WHOI.